ISSN 1810-0384

ADVANCES IN ELECTROMETALLURGY

No. 2 Volume 9 2011

CAMBRIDGE INTERNATIONAL SCIENCE PUBLISHING

Advances in Electrometallurgy is a cover-to-cover English translation of *Sovremennaya Elektrometallurgiya*, published four times a year by International Association 'Welding' at the E.O. Paton Electric Welding Institute, National Academy of Sciences of Ukraine, 11 Bozhenko Street, 03680 Kyiv, Ukraine

Published by

Cambridge International Science Publishing Ltd
7 Meadow Walk, Great Abington, Cambridge CB21 6AZ, England
Tel: +44 (0) 1223 893295; Fax: +44 (0) 1223 894539
email: cisp@cisp-publishing.com; http://www.cisp-publishing.com

Advances in Electrometallurgy 2011 ***9*** *(2) 63–68*
Translated from Sovremennaya Elektrometallurgiya 2011 ***9*** *(2) 3–7*

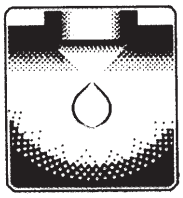

ELECTROSLAG TECHNOLOGY

Using two-circuit electroslag remelting for producing steel-copper blanks for anodes of DC arc furnaces

V.A. Zaitsev, L.B.Medovar, P.I. Tishchenko, B.B. Fedorovskii and V.M. Zhuravel'

E.O. Paton Electric Welding Institute, Kiev; Elmet-Rol, Kiev; Ukrainian Metallurgical Technologies, Donetsk

Abstract Electroslag remelting using the two-circuit diagram (ESR TC) with the replacement of electrodes during melting for producing bimetal ingots is described. The comparison of the effect of ESR TC and standard ESR of composite consumable electrodes on the size of the transition zone of the bimetal ingot is given. The capability of melting of steel–copper ingots of high quality using the technology of ESR TC for producing billets of anodes, i.e. hearth electrodes of d.c. arc furnaces, is shown.

Bimetals are used quite widely in technology because of their unique properties, by which they differ from the components forming them. There is a large number of different methods of production of these materials. Some areas of industry require bimetallic blanks (cast and/or deformed) with a large cross-section. These are bimetallic sheets, large transition pieces for welding dissimilar metals, the rotors of steam turbines with different chemical composition of steel along the length (for low, medium and high pressure stages), steel-copper hearth electrodes (anodes) of arc DC furnaces, and other components for important applications.

Welding (permanent joints) of dissimilar metallic materials in large cross sections is associated with considerable difficulties. To produce bimetallic semifinished products and components with a large cross-section, it is efficient to use electroslag remelting and other electroslag technologies which have been analysed in detail in [1].

Because of the new impetus in the construction of steel melting DC arc furnaces (SMD-CAF), it has become necessary to produce bimetallic steel–copper billets of large dimensions [2]. In particular, the hearth electrodes of the largest arc melting DC furnace in the world (420 t), constructed by the company Danieli in Japan, required the supply of steel–copper billets with a diameter greater than 600 mm [3].

Attempts for producing similar blanks by consecutive electroslag remelting of compound electrodes from dissimilar materials were

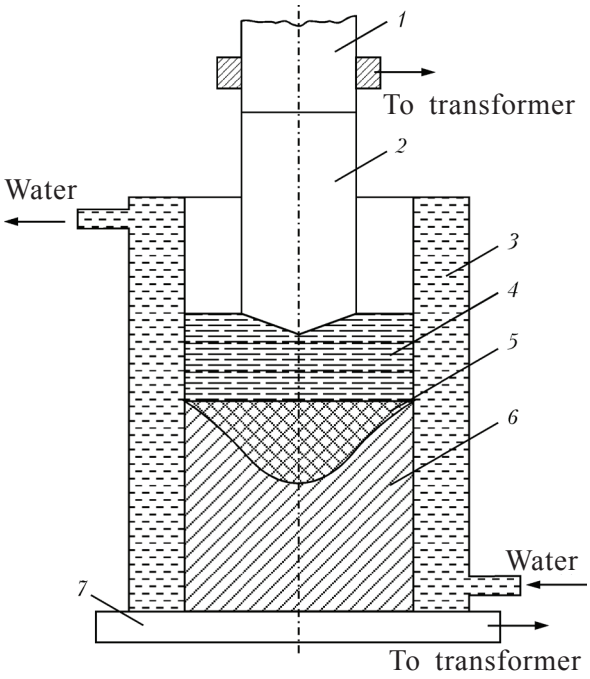

Fig. 1. Diagram of electroslag remelting of a compound consumable electrode: 1) metal B; 2) metal A; 3) solidification mould, 4) the slag pool; 5) metallic pool; 6) billets; 7) baseplate.

described in [4–7] (Fig. 1).

The experience shows that in consecutive melting of the consumable electrode, consisting of two dissimilar metals A and B, the composition of the metal pool changes from the moment of arrival of the first droplets of metal B into the liquid metal pool, formed previously by the molten metal A. The concentration of metal A in the pool gradually decreases, whereas that of metal B increases. Finally, there is a moment at which only the metal B is present in the metal pool. The zone of changes of the composition of the metal from A to B is a transition zone as a result of mutual mixing of these metals. However, as shown in [7], the main shortcoming of the method – the large length of the transition zone – became evident already in the initial stages of development of the method. Experiments carried out in 1967 determined the length and composition of the transition zone in the electroslag remelted ingots, produced from the compound consumable electrode, under the condition that the volume of the liquid metal pool at the moment of melting of the second part of the electrode is completely stabilised. In this case, a transition zone forms in the bimetallic billets produced by electroslag remelting, and the relative composition C' of the zone changes in accordance with the exponential law:

$$C' = e^{Vg/V0},$$

where V_g is the volume of metal 'grown' from the moment of melting of the second part of the electrode; V_0 is the initial volume of the liquid metal pool.

It can be easily calculated that in remelting the compound electrode consisting of the metals A and B, it is necessary to melt of the metal B in the volume equal to $5V_0$, to ensure that the resultant metallic pool consists of 1% of metal A and 99% of metal B. In other words, the length of the transition zone in this case is equal to approximately 5 depths of the metal pool. On the condition that the thickness of the metal pool is equal to approximately half the diameter of the billets, the size of the transition zone equals 2.5 times diameter of the billets which is a relatively large size, not acceptable in practice.

If the volume of the liquid metal pool continuously increases during melting of the billets, the composition of the transition zone is formed by another mechanism. It was shown in [8] that the composition of the transition zone in these conditions changes in accordance with the following law

$$C' = \left(V_c / V_0\right)^{-s}, \quad S = u / \left(u - 1\right),$$

where V_c is the current volume of the liquid metal pool; u is the ratio of the melting rate of the billets and the solidification rate.

This expression shows that the length of the zone with variable composition depends on the ratio of the melting and solidification rates and decreases with increase of this ratio, and it depends also on the volume of the metal pool, existing at the start of melting of the second part of the electrode. As shown by the practice and calculations of

the standard process of electroslag remelting, it is not possible to reduce greatly the size of the zone of variable composition by varying these parameters in rational ranges [9]. In addition, electroslag remelting of the compound electrode produces the transition zone only with a small is transition from one metal to another.

Attempts have been made to overcome these difficulties in electroslag remelting by replacing the electrodes during remelting. However, in this case, it is not possible to reduce greatly the depth of the metal pool. However, if the replacement of the electrode carried out to produce a short transition zone results in partial solidification of the metal of a specific composition prior to the start of melting of the metal of another composition, the formation of unacceptable defects is unavoidable.

The method of electroslag remelting by the two-circuit scheme (ERTCS), developed at the E.O. Paton Electric Welding Institute, Kiev, eliminates these shortcomings [10]. Figure 2 shows the principal diagram of the method.

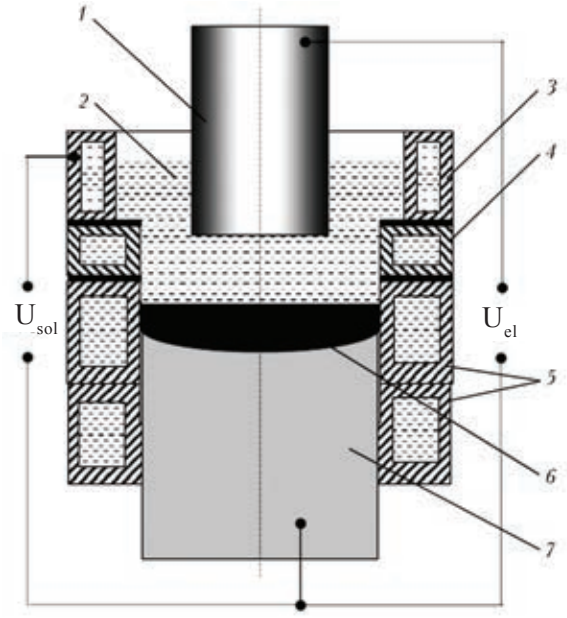

Fig. 2. Diagram of two-circuit electroslag remelting: 1) consumable electrode; 2) slag pool; 3) current-conducting section; 4) separation section; 4) shaping section; 6) metal pool; 7) ingot.

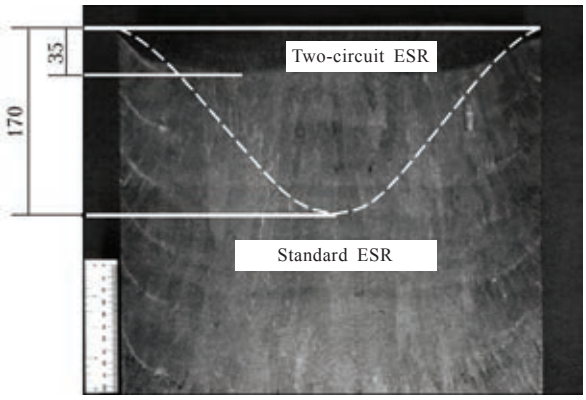

Fig. 3. Profile of the metal pool in two-circuit electroslag remelting of a billet with a diameter of 350 mm (the broken line shows the profile in standard electroslag remelting).

The results of a large number of experiments show that in this method of electroslag remelting, the relationship between the electrical power, introduced into the slag pool, and the melting rate of the ingot is violated. This means that in ERTCS it is possible, in comparison with standard electroslag remelting, to vary the rate of melting of the billets and, correspondingly, the depth of the liquid metal pool. Thus, ERTCS similar to cold hearth remelting processes. Figure 3 shows the sulphur print of a billet with a diameter of 350 mm, illustrating the possibilities of using ERTCS for controlling solidification.

The possibilities of ERTCS for producing billets with the chemical composition variable along the length of investigated on steel and alloys with a wide solidification range. In particular, simulation bimetallic billets with a diameter of 350 mm were produced. In the billets, a high-speed steel and a nickel alloy were welded to low carbon steel. Both these materials are characterised by a wide solidification range. The application of ERTCS resulted in the formation of a transition zone in these billets shorter than 100 mm. The distribution of the main chemical elements along the fusion line is shown in Fig. 4 [9].

The experimental results were considered in making the decision on the application of paste that for producing steel–copper bimetallic billets as blanks for the production of anodes for arc steel melting DC furnaces. It

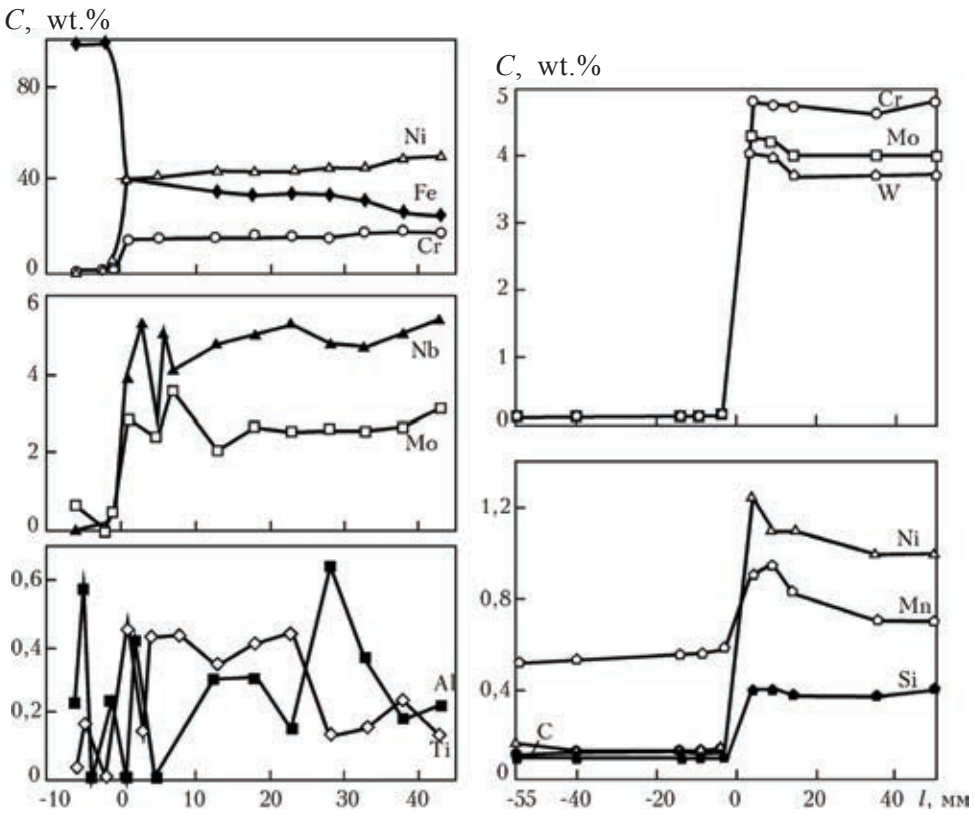

Fig. 4. Distribution of the main chemical elements in the vicinity of the fusion line of bimetallic billets, produced by ERTCS; C) the content of the elements; l) the distance from the fusion line.

was attempted to use electroslag remelting of the compound steel–copper consumable electrode for producing these blanks which were regarded as unsuitable because of the formation of a long transition steel–copper zone.

The anode (hearth electrode) is the main element of the arc steel melting DC furnaces [2]. The design of the anode should ensure efficient cooling, reliability of electrical contact with the charge at the minimum heat losses and a simple and technologically efficient production method. The material of the hearth electrode should be selected taking into account reliable operation at high thermal and current welding, the resistance to mechanical and thermal shocks, the purity of the melt and absence of interaction of the melt with the lining of the furnace.

Thus, these factors determine the main requirements on the design of the anodes - efficient electrical contact and high stability.

In the Ukrainian industry, the arc DC furnaces use mostly the rod-shaped steel–copper, hearth electrodes (Fig. 5). The upper steel part of such an electrode is in contact with liquid metal and partially melts during opera-

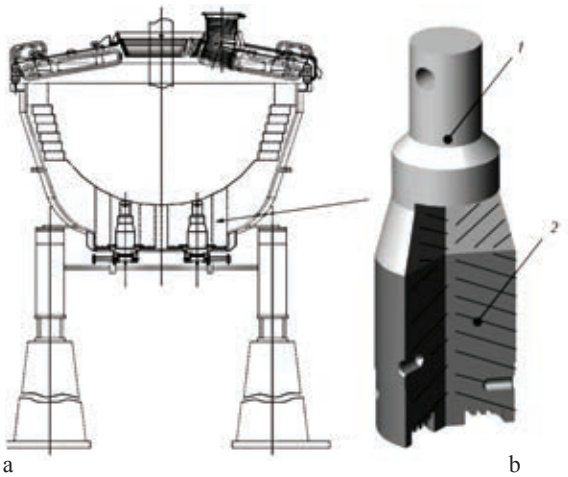

Fig. 5. Position of two hearth electrodes in a 12 t DC arc furnace (a) and the model of the hearth electrode with thie cross section in the body (6) [11]; 1) steel; 2) copper.

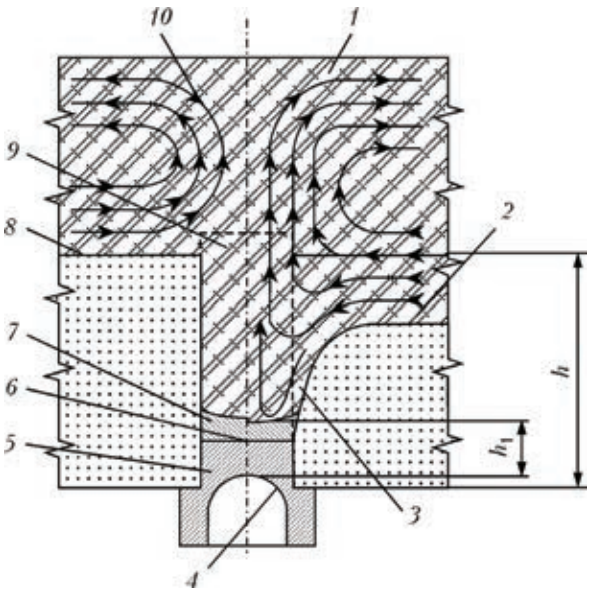

Fig. 6. Diagram of the operation of the hearth electrode in a DC arc furnace [12]: 1) liquid pool; 2) refractory lining after wear; 3) anode pit; 4) water cooling of the electrode; 5) copper part of the electrode; 6) steel–copper joint; 7) unmelted steel part of the electrode; 8) the initial refractory lining; 9) initial steel part of the electrode; 10) liquid steel flows.

tion, and the lower copper part is situated below the melting zone and is cooled with water (Fig. 6).

Previously, the hearth electrodes of this type were produced from separately rolled copper and steel blanks joined together by manual welding, after machining to the finish dimensions. This technology of production of the hearth electrodes is associated with difficulties. The physical–mechanical properties of the components of the steel–copper by metal differed. In addition, the steel and copper are characterised by limited solubility in the solid state, poor wetting in the liquid state and by greatly differing solidification temperatures. All these factors greatly restricts the possibilities of joining these metals by conventional welding methods.

The experiments with the application of two-circuit electroslag remelting were carried out in an USh-149 pilot-plant furnace, working with the replacement of the electrodes. The furnace was modified for operation by the ERTCS method. The second circuit of the power mains for the current-conducting solidification mould was connected with a 720 kV·A power source. The billets were melted using steel St3sP and copper M1. The process was initiated by the 'liquid start'. The special slag for remelting of dissimilar materials is based on the standard ANF-28 slag.

The process of ERTCS of the steel–copper billets with the replacement of the electrodes during remelting was carried out using the following procedure. After inducing the slag pool in the solidification mould using the electrical circuit between the current-conducting solidification mould and the baseplate, the steel consumable electrode was introduced, the second electrode-baseplate circuit was activated and the process of ERTCS with withdrawal of the billet started. After remelting the steel electrode with the given length, the electrode–baseplate electrical circuit was opened, the stub was taken out of the slag pool and replaced with a copper consumable electrode.

During the replacement of the steel stub by the Cu consumable electrode increasing the power in the current-conducting solidification mould–baseplate electrical circuit resulted in electroslag heating of the surface of the top

Fig. 7. Withdrawal of a steel–copper billet from the solidification mould.

part of the billets so that it was possible to ensure the efficient formation of the billets. Subsequently, the copper consumable electrode was introduced into the slag pool, the electrode–baseplate circuit was activated and the electrode was remelted by ERTCS up to the formation of a billet of the required length. The process was controlled automatically.

An experimental batch of steel–copper billets with a diameter of 350 mm, 1000–1300 mm long, with the approximately equal length of the steel and copper parts, was produced. The process of withdrawal of the bimetallic billets from the solidification mould is shown in Fig. 7.

The electroslag ingots were accepted after machining in a lathe to the finish state, with 10–15 mm per side. Slag inclusions, pores, discontinuities, lack of fusion defects, cracks and other defects were not allowed in the parent metal and in the transition zone (in particular).

The hearth electrodes for the arc DC furnaces were subsequently produced with a charge of 0.5–12.0 t from steel–copper billets, melted by the ERTCS with the replacement of the electrodes in the melting process, and are used successfully in important applications.

References

1. Paton, B.E., Spets. Elektrometallurgiya, 1973, No. 20, 3–9.
2. Zaitsev, V.A. and Medovar, L.B., Sovremennaya Elektrometallurgiya, 2009, No. 2, 3-8.
3. www.danieli.com.
4. Chekotilo, V.L., et al., In: Proceedings of the Third national conference on electroslag remelting, part II, 1969, 401–407.
5. Nikitenko, E.L., et al., Tsvetv. Metally, 1981, No. 5, 5–10.
6. Paton, B.E., et al., Probl. Spets. Elektrometall., 1980, No. 12, 3–5.
7. Medovar, B.I., et al., Spets. Elektrometall., 1973, No. 9, 9–12.
8. Tsykulenko, A.K., et al., ibid, 2000, No. 3, 1
9. Tsykulenko, A.K., Probl. Spets. Elektrometall. 1993, No. 1, 3–9.
10. Tsykulenko, A.K., Probl. Spets. Elektrometall. 2000, No. 3, 16–20.
11. www.round.com.ua/index.php.
12. Tishchenko, P.I., et al., Naukovi pratsi DonNTU, Metalurgia, 2010, No. 12, 164–179.

Submitted 17.05.2011

Advances in Electrometallurgy 2011 ***9*** *(2) 69–72*
Translated from Sovremennaya Elektrometallurgiya 2011 ***9*** *(2) 8–11*

Investigations of special features of heat generation in the slag pool in electroslag casting with melting-on

A.F. Muzhichenko, M.A. Poleshchuk and V.L. Shevtsov

E.O. Paton Electric Welding Institute, Kiev

Abstract Using the three-dimensional mathematical model, the peculiarities of distribution of the volume heat source in the slag pool during electroslag casting with melting-on of billets of stop valve bodies were investigated. It was found that additional zones of increased heat evolution are formed near the edges of pipe branches being melted-on. The dependence of the intensity of heat evolution in these zones on the technological parameters of the electroslag process and geometry of the melting space was defined.

Valves with the efficient transmission section from 50 to 100 mm and thick flanges at the end of the nozzle work at high pressure (up to 70 MPa) and are of the main elements of equipment used for the extraction of oil and natural gas from large depths. The bodies of these valves were previously produced from forgings or stampings. The currently available technology of production is labour-consuming, expensive and requires unique pressing equipment [1,2].

The E.O. Paton Electric Welding Institute, Kiev has developed, as an alternative, a method of electroslag casting with melting-on (ESCMO) of the blanks of bodies of flange valves in which only the central part of the body is melted with simultaneous melting-on of previously produced branches with massive flanges at the ends [3,4].

Investigations of the mechanical properties of different parts of the bodies of the flange valves, produced by these methods, shows that as regards the strength properties, the metal of the cast electroslag bodies is not inferior to the deformed metal and has higher ductility properties [5].

However, in the course of experimental melting it was established that the zone of joining the branch with the central part of the body may contain lack of fusion defects and cracks. It was assumed that the formation of these defects is determined by the distribution of current and, therefore, heat generation in the volume of the slag pool.

To verify this assumption in melting of the blanks of the body of the valves with the effective diameter of 50 mm, it was necessary to carry out special experiments. Prior to the start of melting, one of the branches was connecting directly with the baseplate by a current-conducting 'bridge', and the other one was electrically insulated from the wall of the solidification mould and, consequently, the passage of electric current through it was completely prevented (Fig. 1).

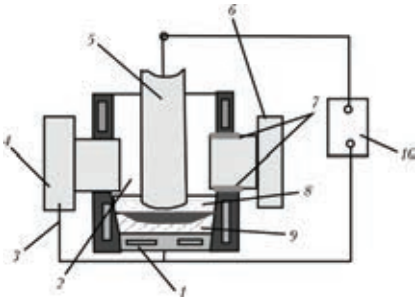

Fig. 1. Experimental setup for evaluation of the relationship of the quality of melting-on of the branches and current distribution in the slag: 1) baseplate; 2) solidification mould; 3) current-conducting bridge; 4) non-insulated branch; 5) consumable electrode; 6) insulated branch; 7) electrical insulation; 8) slag pool; 9) melted blank; 10) power source.

The quality of joining the branches with the central part of the body obtained in the experiments varied (Fig. 2). A uniform fillet formed between the non-insulated branch and the baseplate with the given radius over the entire perimeter (Fig. 2a). At the same time, there was no fillet at the insulated branch and a layer of slag skull forms between its side surface and the central part of the body of the valve (Fig. 2b).

Thus, the experiments show that the working current, passing through the branch, has the controlling effect on the quality of melting-on. This current influences the heat generation in the slag pool in the zone of the branches, forming a fillet over the entire perimeter.

The level of currents, flowing through the branches and, consequently, a generation in the slag in the vicinity of the ends depend on many factors, including on the electrical resistance of individual sections of the slag pool, the mutual distribution and geometrical dimensions of the current-conducting parts (consumable electrode, branches, solidification mould and slag pool), and also the technological parameters of the process of ESCMO. The effect of these factors on the process of heat generation in the slag pool can be described by mathematical modelling.

For this purpose, the authors developed a mathematical model of current and heat generation in the slag pool. In ESCMO during direct melting-on, when the level of the slag pool during melting of the consumable electrode rises along the ends of the branches, the conditions of heat supply from the slag to the side surface of the melting space of the tent greatly not only on the height of the level of the slag but also on the angle of rotation of the radius around the axis of the melted blank.

The slag pool is characterised by the formation of new directions of current passage from the consumable electrode through the slag to the ends of the branches, shunting the working current, passing through the consumable electrode. The experiment shows that the total values of these shunting currents may reach 50% of the working current.

In [6] tasks and boundary conditions were formulated, and the results of modelling and distribution of the current of heat sources at different moments of the ESCMO process were presented.

The experimental results show that at the start of melting-on, the distribution of the volume heat sources in the slag pool greatly changes. During the passage of the slag pool along the ends of the branches, facing the melting space, new additional zones of high-intensity heat generation in the slag form in their vicinity. At a specific moment of time, the power of each zone may reach 10% of the power of heat generation in the region below the electrodes. Consequently, the ends

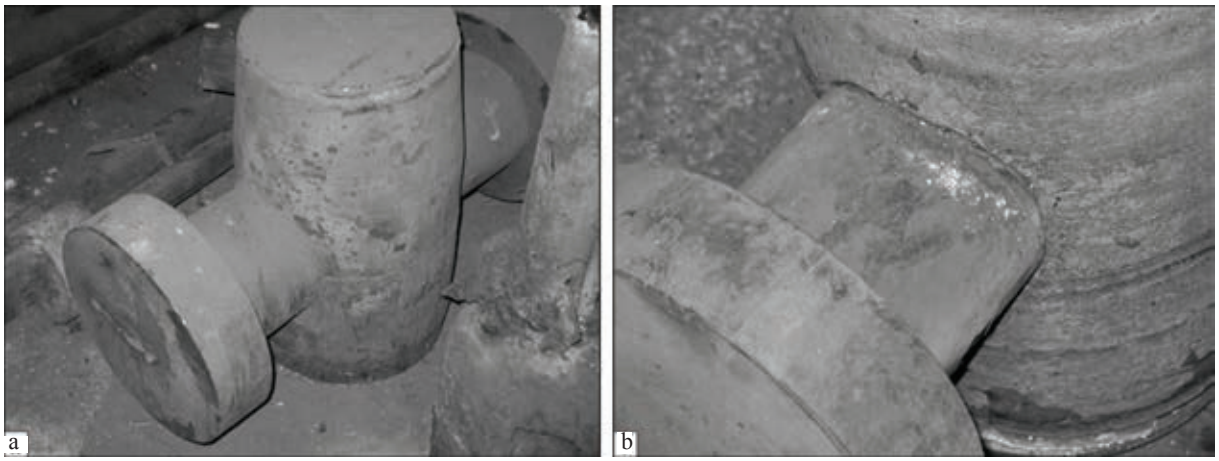

Fig. 2. External appearance of the joint of the central part of the body of the valve with the non-insulated (a) and insulated (b) branches.

of the branches, electrically connected with the baseplate, are heated at a higher rate, melt and form high-quality joints with the melted part of the blank.

The results of investigation of the distribution of the power of volume heat sources in the slag pool in the vicinity of the ends of the branches in relation to the geometrical dimensions of the blanks and the technological parameters of the ESCMO process, obtained by mathematical modelling, described in [6], will be presented.

Figure 3 shows the distribution of specific heat sources in the slag pool in paste that of the blanks of the bodies of Du-80 and DU-50 valves and the moment when the surface of the metal pool approaches the lower edges of the branches. The blank of the body of the Du-80 valve contains branches with a diameter of 160 mm and is melted in a solidification mould with the diameter of 270 mm.

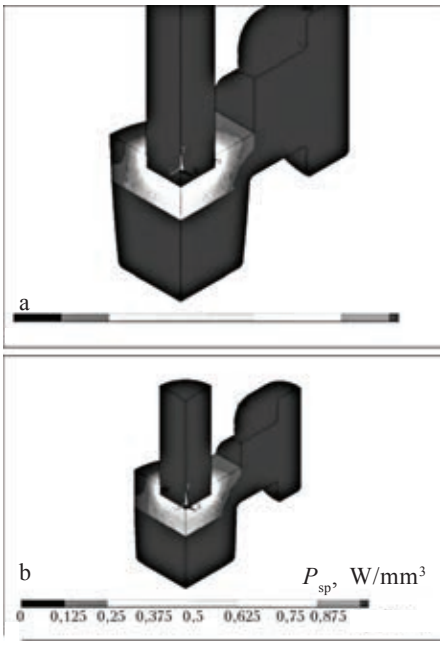

Fig. 3. Distribution of specific heat sources Psp in the slag pool in ESCMO of the blanks of the bodies of the valves D u-80 (a) and Du-50 (b).

In melting the blanks of the body of the Du-50, the diameters of the branches, adjacent to the central part of the bank of the body of the valve, were 120 and 240 mm. Calculations were carried out with the same values of the power generated in the slag pool and the depth of the slag pool (75 mm).

As indicated by Fig. 3, at the same values of the specific power, the intensity of heat generation in the vicinity of the ends of the branches is approximately the same. The power, generated in the slag pool with a constant chemical composition, situated in a specific solidification mould, can be controlled by changing the voltage of the power source or the depth of the slag pool. The effect of these parameters on the intensity of additional heat sources in the vicinity of the ends of the branch is shown in Fig. 4.

The effect of the diameter of the branches on the intensity of heat generation in the vicinity of the ends of the branches was investigated separately for the blanks of the bodies Du-80 and Du-50). The simulation results are presented in Fig. 5.

As shown by Fig. 5, a reduction of the

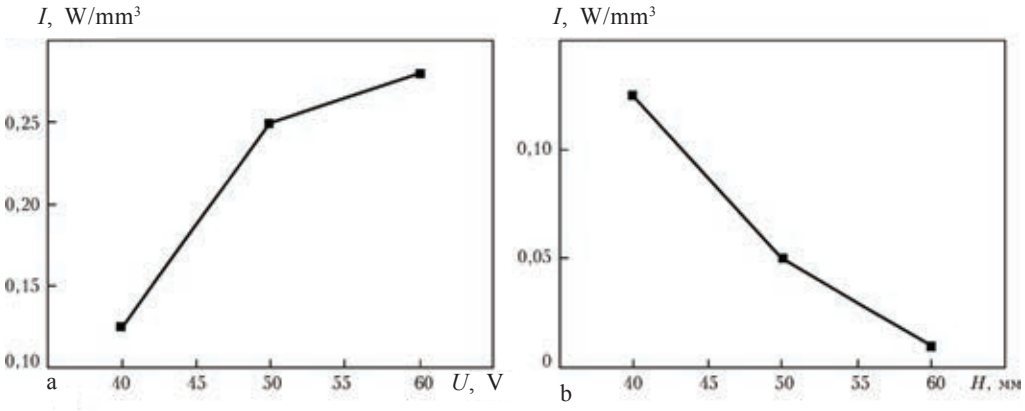

Fig. 4. Dependence of the intensity *I* of additional heat generation at the edges of the branches on voltage in the slag pool *U* (a) and its depth *H* (b).

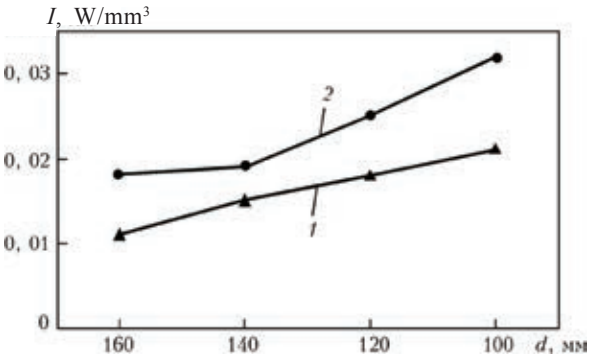

Fig. 5. Dependence of the intensity *I* of heat generation in the vicinity of the ends on the diameter *d* of branches: 1) Du-80; 2) D u-50.

diameter of the branch increases the intensity of regeneration in the vicinity of its melted-on end. This additional heat generation increases the depth of penetration of the end of the branch, indicated by the macrostructure of the zone of joining of the branches of the blanks of the bodies of the valves with the effective transmission diameter of 50 (Du-50) and 80 mm (Du-80) (Fig. 6).

Thus, as a result of mathematical modelling, we determine the dependence of the intensity of heat sources in the additional heat generation zone, formed in the slag pool in the vicinity of the ends of the melting-on branches, on the technological parameters and geometry of the melting space.

The resultant relationships can be used in the determination of the technological conditions of the process of ESCMO in melting the bodies of the valves of different standard dimensions.

References

1. Vaisberg, G.L. and Rimchuk, D.V., Safety. Questions and answers, Kharkiv, 2002.
2. Steel forgings instead of steel castings, Advertising literature of Cameron company, Neftegaz-90 exhibition.
3. Poleshchuk, M.A., et al., Sovremennaya Elektrometallurgiya, 2009, No. 2, 13-17.
4. Poleshchuk, M.A., et al., Armaturostroenie, 2009, No. 4, 49–54.
5. Poleshchuk, M.A., et al., Sovremennaya Elektrometallurgiya, 2009, No. 8, 8-12.
6. Muzhichenko, et al., Sovremennaya Elektrometallurgiya, 2010, No. 2, 17-20.

Submitted 16.02.2011

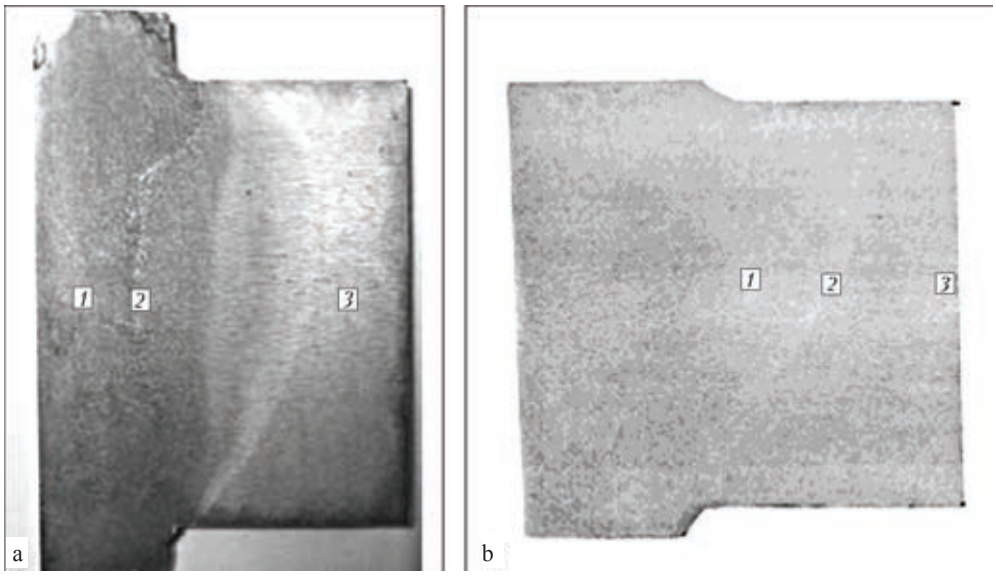

Fig. 6. Macrosections of the zones of joining of the branches with the cast body of the valves Du-80 (a) and Du-50 (b): 1) cast electroslag metal; 2) fusion line; 3) the heat affected zone in the metal of the branch.

Advances in Electrometallurgy 2011 ***9*** *(2) 73–77*
Translated from Sovremennaya Elektrometallurgiya 2011 ***9*** *(2) 11–15*

Criteria for selecting the design of casting moulds for centrifugal electroslag casting

S.V. Skripnik and D.F. Chernega

Kiev Polytechnical Institute

Abstract Criteria of the selection of design of metallic non-cooled mould, the main of which are material, method of mould manufacture, level of centrifugal forces, geometric parameters of casting, are considered. Options of the design of casting moulds are described for producing castings, both simple and intricate in configuration.

Special attention is paid to the problems of energy efficiency of the production of engineering components because of the continuous increase of the price of energy carriers. Cast blanks appear to be the cheapest and most efficient of components when using low-deformability and low-weldability creep-resisting steels and alloys. The delaying factor of extensive application of the cast components, especially in gas turbines, are the stringent requirements on the quality and properties.

The E.O. Paton Electric Welding Institute, Kiev, has developed a method of centrifugal electroslag casting for producing high-quality components/blanks with the properties similar to those of forged components [1]. In the production of engineering components by the methods of centrifugal electroslag casting, the metal, produced in electroslag crucible furnaces, is poured into casting moulds, rotating around a vertical axis, together with the slag used in melting. The melt, accumulated in the crucible, can be poured into a single- or multiposition casting mould, fixed to a rotating plate, to produce the appropriate number of castings.

The casting moulds in centrifugal electroslag casting have the form of metallic and cooled shapes (ingot moulds). A combined casting mould – an ingot mould and a ceramic bar – or a faced ingot moulds with different thickness of the coating for each shaping elements and the amount, can also be used.

The main task in the design of ingot moulds is the selection of material and thickness of the working walls. These parameters of the design determine the durability of the casting mould -– resistance to cracking and distortion.

The most widely used materials for the manufacture of large ingot moulds for centrifugal electroslag casting are carbon steels 10, steel 20, 25L, St 3 and high-strength cast iron VCh 42-12, VCh 45-5. The advantage of the cast iron moulds is higher resistance, in comparison with the steel moulds, and a shortcoming is complicated repair. The currently available methods of it training cast iron ingot moulds by welding (with the exception of welding in the heated condition) do not ensure the formation of the deposited metal with the uniform structure and properties of the layer.

The steel cast or welded ingot moulds, in contrast to the cast iron moulds, can be repaired many times by welding defects and by surfacing. The process of repair by welding in simple, and efficient preparation of the areas to be welded up is essential.

The selection of the method of production of the ingot moulds depends on many factors: overall dimensions and configuration of the casting, accuracy standards, material and

production capacity of the plant.

The heat treatment of the casting mould in the production of steel cast iron blanks for the ingot moulds is compulsory. This is determined by the need to change the cast structure, and also relieve the residual technological (casting, welding, etc) stresses. The residual stresses may cause fracture of the working wall of the mould or its distortion as a result of stress relaxation [2].

It is assumed that the wall thickness of the ingot moulds X_2 should be equal to the depth of heating the mould at the end of solidification of the casting. If the value of X_2 is higher, the thermal conditions of formation of the casting do not change.

There are several methods of calculating the wall thickness of the mould, but none of the methods is universal. In the first approximation, the following empirical relationships are recommended, for example: $X_2 = 13+0.6\ 2X_1$ [2]; $X_2 = 11\sqrt{2X_1}$ [3], where X_1 is half the thickness of the wall of the casting.

On the basis of the theoretical analysis of the stress–strain state of the working walls of the ingot of different design the value of X_2 for the cylindrical ingot moulds (Fig. 1a) for the hollow castings is accepted on the basis of the criterion X_1/R_1, where R_1 is the outer radius of the casting [4, 5]. The positive moments in this case is that the configuration of the mould is taken into account by means of the outer radius of the casting. However, the ingot moulds, calculated using this method, are relatively massive and cumbersome.

According to GOST 1 6 to 37-70 standard, the value X_2 is determined using a graph (Fig. 1b). For the steel working walls and high-strength cast iron, the value X_2 is closer to the lower boundary of the crosshatched region. Calculation of the wall thickness of the casting mould by these variants produces the average value and optimum design solution can be taken.

It is necessary to take into account the fact that the pouring of metal with slag into the rotating moulds is accompanied by the formation of a heat-insulating slag skull layer on the walls of the working cavity. The skull layer absorbs a large part of thermal loading. This is accompanied by a reduction of thermal stresses in the mould walls with no increase of the service life.

The reduction of the thermal stresses makes it possible to reduce the war thickness of the mould in design. On the other hand, in centrifugal electroslag casting the casting mould is loaded by the effect of the force centrifugal field.

Depending on the design and service re-

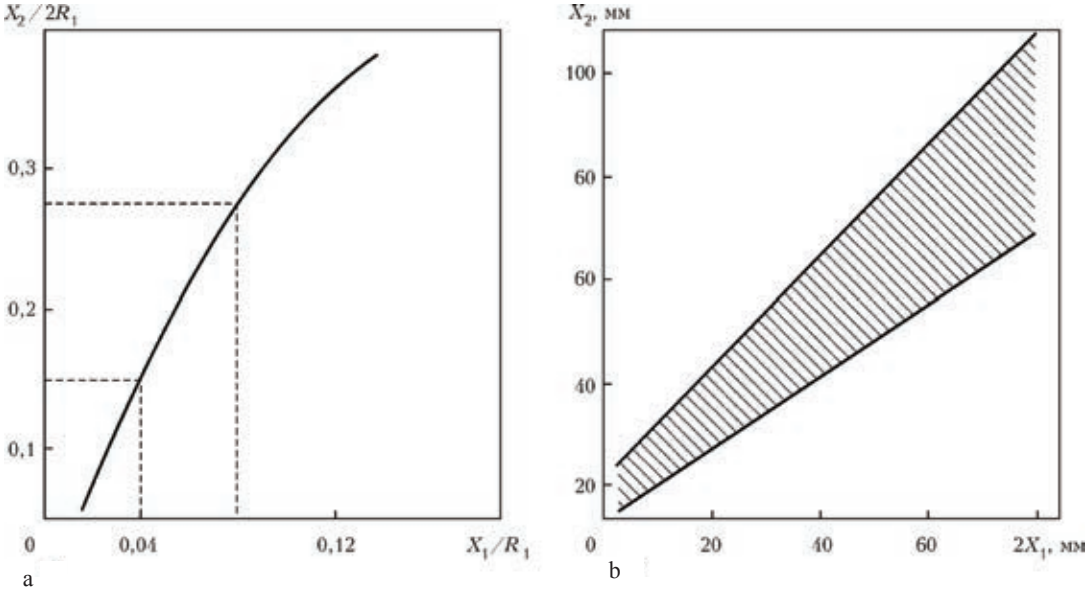

Fig. 1. Dependence $X_2/2R_1$ on X_1/R_1 (a) and X_2 on $2X_1$ (b): X_1 is the half thickness of the wall of the casting; X_2 is the half thickness of the wall of the ingot moulds; R_1 is the outer radius of the casting.

quirements on the configuration and quality of the casting, the gravitational coefficient may vary in a wide range (up to 100 or more units). The mass of liquid metal and slag increases by the same amount under the effect of centrifugal forces. Therefore, the strength of the casting mould after preliminary selection of the wall thickness must be calculated, as in the case of pressure vessels.

In the final analysis, the design of the mould depends on the level of working stresses, complexity and the rigidity of the component, and also on the required safety.

The simplest the design has the form of 'shaken-out' ingot moulds with a horizontal separation plane (Fig. 2). They can work for long periods of time without shrinking or distortion. The service life of these moulds depends mainly on the mass of the produced castings: as the mass and size of the casting increases, the service life becomes shorter.

To produce castings of complicated configuration, it is recommended to use sectional ingot moulds with the vertical (Fig. 3) and horizontal (Fig. 2) splitting planes. They ensure rapid extraction of the solidified casting. The wall thickness of these ingot moulds should be increased in order to reduce the distortion susceptibility of the individual sections. After a specific number of castings, it is necessary to machine the cavity of these moulds to some depth to ensure easy extraction of the castings. This is accompanied by a small increase of the allowance for machining of the cast components.

The casting, shown in Fig. 3, is characterised by the difference in the wall thickness. Therefore, to form the conditions for uniform solidification of the walls, a layer of an insulating coating must be deposited on the thin wall elements of the casting.

The method of centrifugal electroslag casting makes it possible to produce components of almost any configuration, for example, sprockets for drive chains. In this case, the ingot moulds contains individual sections, forming the teeth of the sprocket (Fig. 4).

To produce several castings of relatively small height, it is recommended to use a multiposition mould consisting of the appropriate number of identical shaping elements and a dosing pocket in the upper part of the mould. The pocket is used for receiving the excess amount of metal poured from the crucible into the multiposition rotating moulds (Fig. 5).

The special features of the casting properties of the steel require a different approach in comparison with that used in other cases. The steel is poured at a high-temperature and is characterised by large shrinkage and solidification, and has a low level of fluid-

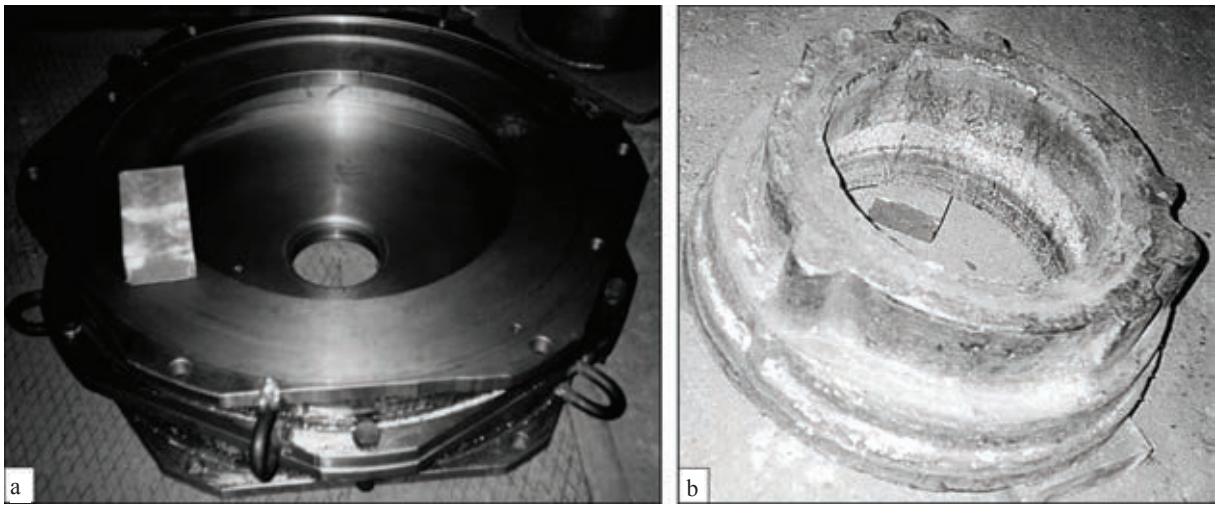

Fig. 2. Whole 'shaken-out' single-position ingot moulds for centrifugal electroslag casting (a) and the blank for a gearwheel of MAZ quarry dumper (b).

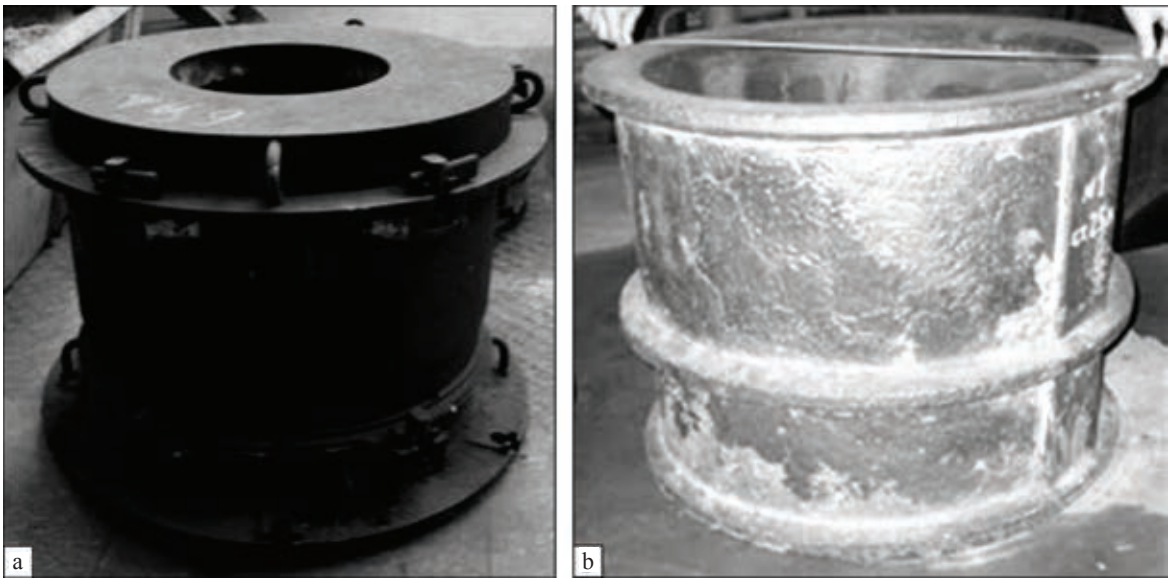

Fig. 3. Sectional single-position ingot moulds for centrifugal electroslag casting (a) and the blank for a gas turbine (b).

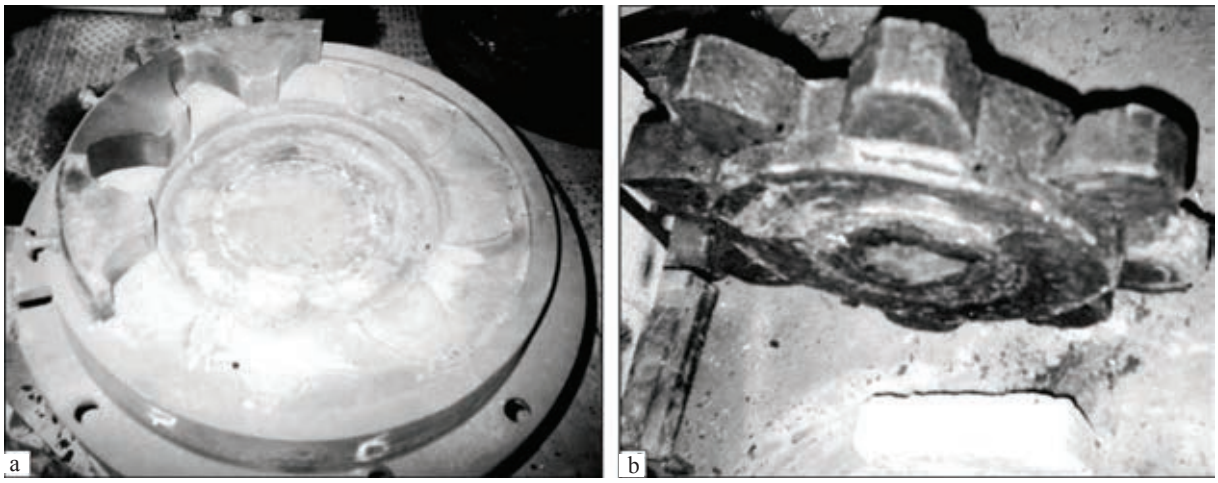

Fig. 4. Sectional single-position ingot moulds for centrifugal electroslag casting (a) and a cast blank of a ??? (b).

ity and higher crack formation resistance. Therefore, when producing the steel castings of a complicated shape, it is irrational to use combined metallic moulds with the layer of the heat shielding coating of different thickness on the individual shaping elements. Thus, it is easy to regulate the heat removal into the side walls of the mould, the ends and shaping cavities, and ensure simultaneous solidification of the walls of the castings of different thickness. This is accompanied by a reduction of the probability of formation of hot and cold cracks in the casting.

For the casting characterised by the presence of thermal sections, the latter can be removed using flexible rods, secured in the appropriate part of the mould (Fig. 6). The thickness of the casting in the individual sections is equalised and this has a beneficial effect on solidification.

The rods contain a metallic axis with wedge fixing and a support disc, and also a sleeve made of a rod shaped refractory mass with small convexity (Fig. 7) which are placed in the mould in assembling. The ring-shaped gap between the axes of the rod and the sleeve ensures compliance.

This case, the frequency of rotation of

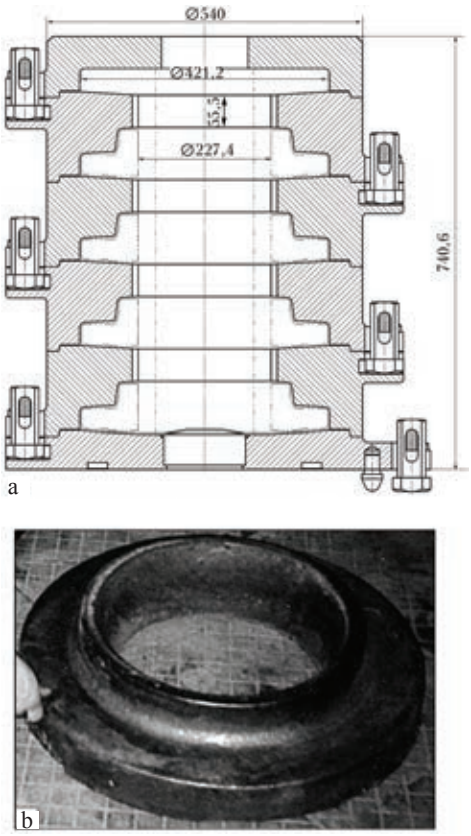

Fig. 5. Design diagram of a multiposition 'shaken-out' ingot mould with a dosing pocket (a) and a cast blank of a flange of a pipeline (b).

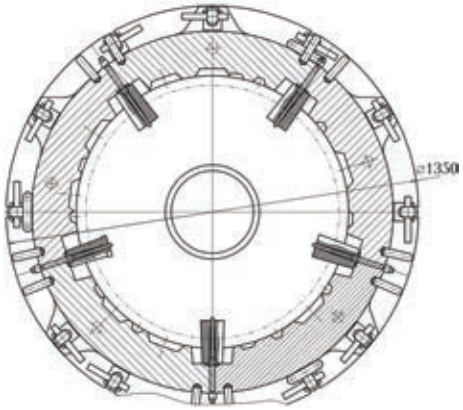

Fig. 6. Diagram of a sectional ingot moulds with rods produced from a compliant material, placed in shaping cavities.

the mould is the turning in relation to the permissible pressure of liquid metal, preventing failure of the rod. The strength of the rod material in centrifugal electroslag casting should not be lower than $(12…15) \cdot 10^2$ kPa. The rods are removed by knocking them out in the direction of the casting axis.

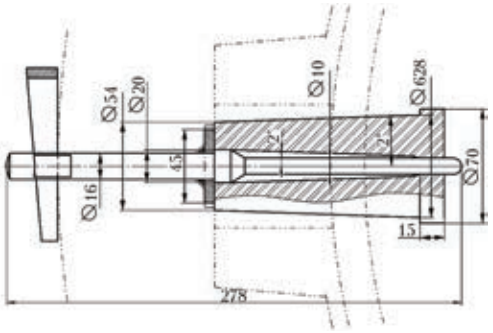

Fig. 7. Diagram of a combined rod placed on the axis of the thermal section.

Conclusions

1. The ingot moulds for centrifugal electroslag casting our components for most important applications from the viewpoint of both the production of high-quality products and industrial safety and labour protection and, consequently, the latest achievements of science should be used when designing these moulds.

2. A promising method of producing the blanks for the steel ingot moulds is electroslag casting which produces high density, isotropic blanks, with high impact toughness at high temperatures. This is one of the main factors of the stability of the steel ingot moulds [3].

3. A promising method of producing the blanks for steel ingot moulds is the methods of centrifugal electroslag casting which produces bimetallic blanks with an internal layer made of a creep-resisting alloy, for example KhN78T (EI435) which, necessary, should be welded up or deposited with widely used creep resisting OZL-25B electrodes with the same composition.

References

1. Medovar, B.I., et al., Centrifugal electroslag casting, Znanie, Kiev, 1983.
2. Emel'yanov, A.A., Technology of the casting mould, Mashinostroenie, Moscow, 1979.
3. Veinik, A.I., Casting into ingot moulds, Mashinostroenie, Moscow, 1980.
4. Serebro, V.S., Izv. VUZ, Chernaya Metallurgiya, 1968, No. 11, 163–167.
5. Serebro, V.S., Mathematical investigation of the cooling of casting and faced ingot moulds, in: Casting properties of alloys, Institute of Problems of casting, Academy of sciences of the Ukrainian SSR, Kiev, 1972, 43-44.

Advances in Electrometallurgy 2011 ***9*** *(2) 78–81*
Translated from Sovremennaya Elektrometallurgiya 2011 ***9*** *(2) 16–18*

ELECTRON BEAM PROCESSES

Production of high-quality nickel ingots-slabs by electron beam melting

N.P. Trigub, V.. Berezos, V.D. Korniichuk abd Yu.A. Mosunov

E.O. Paton Electric Welding Institute, Kiev; TekhMetSplav, Ufa

Abstract: The results of experimental investigations of the melting of nickel scrap by electron beam melting are presented. A technology is developed for producing high-quality nickel ingotsûslabs.

As a result of the development of new structural materials in which the nickel is the main alloying element, the demand for these materials is continuously increasing.

The main users of nickel are the metallurgical, power engineering, chemical and other branches of industry. Pure nickel is used for the manufacture of various equipment, devices, boilers and crucible is with high corrosion resistance and constant physical properties. Of special importance are nickel materials in the manufacture of containers and holders for the the requirements of power engineering and chemical industries.

Ukraine has only a small deposits of nickel ores which are being exhausted quite rapidly. In particular, the reserves of nickel deposits and the Lipovenkovskoe deposit in the central Ukraine could be exhausted within five years [1]. The demand for nickel in Ukraine is almost completely satisfied by imports. Therefore, the development of technology for producing high-quality nickel ingots from scrap is an important task.

The industry, especially power engineering, requires semifinished products from nonferrous metals and alloys with the minimum content of gases and impurities, and also characterised by high density and plasticity. Many of the impurities are harmful, and greatly reduce the physical and chemical properties of the metals and alloys. The development of efficient methods of protection against the penetration of harmful impurities and removal of these impurities during production and further treatment of the metals is one of the main tasks of metallurgy.

Electrolytic refining of nickel, carried out to remove the harmful impurities, produces the metal with relatively high purity (99.90...99.98 %) [2]. However, it is very difficult to maintain this value in the remelting of electrolytic nickel.

The improvement of technology of production of high purity nickel is achieved by melting this material in vacuum induction or arc furnaces. In vacuum induction melting of nickel it is not possible to prevent completely is contamination as a result of interaction with the crucible lining [3].

Vacuum arc remelting excludes contamination of the nickel because it is carried out in a watercooled solidification mould. However, in this method, nickel is not efficiently refined to remove gases and other impurities are not removed [4]. In addition, in vacuum arc remelting there are highly stringent requirements on the consumable electrode is (they should transmit high currents) which can be satisfied only with considerable difficulties in the assembling of electrodes from electrolytic nickel plates [5].

Analysis of different methods of melting nickel ingots shows that the most efficient and economically justified method of producing special purity nickel ingots by utilising nickel scrap is the technology of electron beam melting (EBM) ensuring the highest degree of refining of nickel with the smallest losses [4]. The method utilises almost completely the waste in the form of sheet cuttings, pieces of waste and shavings. That is no need for carrying out difficult operation such as the production of a compact consumable electrode.

The E.O. Paton Electric Welding Institute, Kiev has accumulated experience with increasing the purity, improving the structure and properties of nickel by electron beam melting [4].

Experimental investigations were carried out in UE 5812 industrial electron beam equipment [6] in which ingots-slabs with the rectangular cross-section were melted from nickel scrap.

The charge is in the form of nickel scrap in the form of sheets of cathodic nickel of N1 grade, and also nickel shavings, grade NP2. The dimensions of the pieces of scrap did not exceed 10 × 500 × 1000 mm. The surface of scrap was cleaned to remove various types of contamination. The consumable electrode was produced in an nonconsumable box. After shaping the consumable blank, equipment was sealed and evacuated.

In melting, the initial charge was fed continuously at a given rate into the melting zone above the intermediate container where it was melted under the effect of electron beam heating. After filling the intermediate container, the liquid metal was poured into a watercooled copper solidification mould. During melting, the ingot was lowered with a withdrawal mechanism in the semi-continuous mode (after increasing the level of liquid metal in the solidification mould by 10^{-15} mm with a linear speed of $(2…3)\cdot10^{-4}$m/s until the pool reached the previous level). The ingot was withdrawn after every pouring of a liquid metal portion into the solidification mould.

The following technological parameters were controlled in melting: the feed rate of the charge, acceleration voltage, and beam current. The melting rate was regulated by the speed of feed of the initial charge into the melting zone, and the numerical values of the acceleration voltage and beam current were measured with appropriate devices.

Ingots of the required length where melted in the stationary regime. Subsequently, a shrinkage cavity was produced in the top part of the ingot. The ingots were cooled in vacuum together with the furnace. Equipment was opened and the ingot was withdrawn using a shop crane.

Hydrogen and nitrogen do not form compounds with nickel stable at high temperatures [2]. In the molten state, nickel can dissolve a large amount of gases (nitrogen, hydrogen, oxygen) which, precipitating during crystallisation of metal as a result of the rapid

Fig. 1. Gas porosity at the melted end of a nickel ingot in the zone of contact with the walls of the solidification mould.

decrease of the solubility of gases with a decrease of the temperature of liquid metal, results in the formation of pores in the ingots.

As a result of the high cooling rate of the ingot in the vicinity of the walls of the watercooled copper solidification mould in electron beam melting, the gases, dissolved in the liquid metal do not manage to leave the liquid pool and some of them remain in the solidified metal, forming cavities – gas porosity (Fig. 1). In solidification of metal these gases can also interact together with the formation of water vapour switch cannot diffuse through the metal and, consequently, result in the formation of porosity in the ingot. If these gases penetrate into the liquid pool, the reaction of the type NiO +2H = Ni + H_2O, NiO +C = Ni + CO [2] can take place.

In order to prevent the formation of gas porosity in melting of nickel ingots it is necessary to increase the holding time of liquid metal in the intermediate container and the solidification mould. In subsequently melting in the optimised conditions of electron beam melting no gas porosity was detected in the nickel ingots.

The nickel ingots, produced by electron beam melting, where analysed for the content of gases and other impurities (Table 1).

Measurements of the chemical composition of the specimens of the initial nickel charge and of the ingots–slabs after electron beam welding were taken in INA-10 equipment (Leybold-Heraeus, Germany) by mass spectrometry of secondary post-ionised neutral particles.

Analysis of the chemical composition of the melted nickel ingots–slabs shows (Table 2) that many low melting impurities are removed during electron beam remelting and the number of nonmetallic inclusions is also reduced.

Table 1. Gas content of nickel prior to and after electron beam remelting

Charge	State	Mass fraction of gases, %		
		[O]	[N]	[H]
H1		0.004	0.0013	0.0003
		0.0002	0.0003	0.0001
HP2		0.005	0.0022	0.0018
		0.0003	0.0003	0.0001

Fig. 2. External appearance of nickel slabs-ingots.

In electron beam melting of alloys based on nickel the content of zinc, bismuth, lead and other low melting impurities greatly decreases. The mass fractions of silicon and carbon change only slightly.

In electron beam melting, liquid nickel does not wet the walls of the solidification mould and, consequently, the side surface of the ingots remains smooth and shiny (Fig. 2).

The process of electron beam melting of nickel and nickel alloys is characterised by high economical factors. The consumption of electrical energy is 1.0…1.2 kW·h/kg. The ingots do not have shrinkage cavities and are characterised by a considerably higher degree of purity in comparison with industrial nickel grades NP2 (Table 2).

Conclusions

1. The experimental results show that it is promising to use electron beam melting technology for utilising nickel scrap. The efficiency of refining nickel scrap to remove gases and impurities by electron beam remelting has been shown.

2. The method of electron beam remelting was used for melting high-quality nickel ingots with a purity of 99.9 wt.%.

3. A technology has been developed for

Table 2. Chemical composition of nickel ingots

Specimen number	Mass fraction of elements, %							
	C	Mg	Si	P	S	Mn	Fe	Cu
	$1.17\cdot10^{-3}$	$1.32\cdot10^{-5}$	$2.41\cdot10^{-4}$	$1.01\cdot10^{-3}$	$1.69\cdot10^{-4}$	$1.69\cdot10^{-3}$	$1.51\cdot10^{-2}$	$1.09\cdot10^{-2}$
1	$1.06\cdot10^{-3}$	$4.0\cdot10^{-6}$	$1.97\cdot10^{-5}$	$1.63\cdot10^{-5}$	$6.77\cdot10^{-5}$	$6.03\cdot10^{-5}$	$4.41\cdot10^{-3}$	$3.91\cdot10^{-4}$
2	$1.02\cdot10^{-3}$	$2.01\cdot10^{-5}$	$2.09\cdot10^{-4}$	$1.6\cdot10^{-6}$	$8.75\cdot10^{-5}$	$1.45\cdot10^{-5}$	$3.52\cdot10^{-3}$	$4.58\cdot10^{-5}$
3	$1.13\cdot10^{-3}$	$2.3\cdot10^{-5}$	$2.37\cdot10^{-4}$	$1.05\cdot10^{-5}$	$7.42\cdot10^{-5}$	$3.23\cdot10^{-5}$	$1.48\cdot10^{-3}$	$3.24\cdot10^{-4}$
GOST 492-2006	0.1	0.1	0.15	0.002	0.005	0.05	0.01	0.01

Speci-men	Mass fraction of elements, %							
	Zn	As	Cd	Sn	Sb	Pb	Bi	Ni+Co
Initial	$1.05\cdot10^{-3}$	$2.02\cdot10^{-3}$	$1.04\cdot10^{-5}$	$6.95\cdot10^{-5}$	$2.77\cdot10^{-5}$	$1.05\cdot10^{-3}$	$1.2\cdot10^{-6}$	99.718
1	$2.50\cdot10^{-6}$	$6.49\cdot10^{-5}$	$5.80\cdot10^{-6}$	$2.42\cdot10^{-5}$	$7.90\cdot10^{-6}$	$1.05\cdot10^{-5}$	$0.1\cdot10^{-6}$	99.982
2	$1.19\cdot10^{-4}$	$0.30\cdot10^{-6}$	$5.60\cdot10^{-6}$	$1.10\cdot10^{-6}$	$9.50\cdot10^{-6}$	$1.92\cdot10^{-5}$	$0.1\cdot10^{-6}$	99.969
3	$5.30\cdot10^{-6}$	$3.29\cdot10^{-5}$	$7.50\cdot10^{-6}$	$3.54\cdot10^{-5}$	$6.90\cdot10^{-6}$	$2.35\cdot10^{-5}$	$0.1\cdot10^{-6}$	99.921
GOST 492-2006	0.007	0.002	0.002	0.002	0.002	0.002	0.002	–

producing high-quality nickel ingots–slabs by electron beam remelting.

References

1. Levine, R.M., The mineral industry of Ukraine, US Geological Survey, Minerals Information, 2008.
2. Perel'man, F.M. and Zvorykin, A.Ya., Cobalt and nickel, Nauka, Moscow, 1975.
3. Bobylev, A.V., Mechanical and technological properties of metals, a handbook, Metallurgiya, Moscow, 1987.
4. Movchan, B.A., Electron beam melting and refining of metals and alloys, NaukovaDumka, Kiev,, 1973.
5. Utkin, N.I., Metallurgy of nonferrous metals, Metallurgiya, Moscow, 1985.
6. Trigub, N.P., et al., Sovremennaya Elektrometallurgiya, 2007, No. 1, 11-14.

Submitted 20.04.2011

Advances in Electrometallurgy 2011 ***9*** *(2) 82–86*
Translated from Sovremennaya Elektrometallurgiya 2011 ***2*** *(9) 19–22*

Structure of two-phase Cu–NaCl condensates, deposited in vacuum from the vapour phase

Yu.A. Kurapov, S.E. Litvin, G.G. Didikin and S.M. Romanenko

E.O. Paton Electric Welding Institute, Kiev

Abstract: Results of investigation of the structure of condensates of the Cu–NaCl composition, their chemical composition and mass fraction of oxygen depending on the content of copper produced from the vapor phase using electron bean evaporation and condensation in vacuum are given. The effect of the copper content on the phase composition of nanoparticles was studied. The kinetics of comparative changes in the mass of porous Cu–NaCl condensates in heating up to 650°C and air cooling was investigated. The obtained results are studied from the point of view of physical and chemical adsorption.

The nanoparticles, produced by almost all methods, are in the metastable nonequilibrium state. On the one hand, this circumstance complicates the investigation and application of these particles in nanotechnology for the formation of devices with stable operation, and on the other hand, the non-equilibrium state of the system makes it possible to carry out unusual and difficult to predict new chemical transformations. The specific dimensional defects are most evident in small particles where the non-regular dependences of the properties on the particle size are dominant. The activity of the particle in relation to the size of the particle is determined by the varying properties of the particle during interaction with the absorbing reagent [1], with the main reagent for the metallic nanoparticles being oxygen. As a result of the high activity of the nanoparticles of the metals, the existence of the particles in the free form, without interaction with the environment, is possible only in vacuum.

The experimental results show [2,3] that the nanoparticles of copper and copper oxide have the strong antibacterial effect as regards the Gram-negative and Gram-positive bacteria. Further development and preparation of medical means on the basis of the nanoparticles of copper and copper oxide require the selection of the method of synthesis of the nanoparticles which would ensure the formation of different compositions of the nanoparticles based on copper with the required content of the essential structural components. The technology of electron beam evaporation and condensation makes it possible to carry out synthesis of these nanomaterials [4].

The aim of the investigations described in the present article was to study the effect of the copper concentration and annealing temperature on the phase composition of the nanoparticles in the porous matrix of NaCl condensates, produced by vacuum electron beam evaporation and condensation.

Experimental materials and procedure

The nanoparticles in a porous salt matrix were produced by condensation of the mixed molecular fluxes of copper and NaCl in vacuum electron beam equipment [5–7]. The measured surface temperature of the copper cooled substrate in deposition of the vapour flows was 30–50°C, the thickness of the condensates was 125–200 μm. The investigations were carried out on transverse cleavage

sections of the condensates and on a powder produced from the condensate milled in an agate mortar.

The elemental composition and structure of the condensates were investigated in a CamScan scanning electron microscope with INCA-200 Energy x-ray attachment. The phase composition of the nanoparticles was determined using the methods of transmission electron microscopy (in Hitachi H-800 microscope, acceleration voltage 100 kV) and by x-ray diffraction analysis in DRON-3 and DRON-4-07 diffractometers in the CuK_α irradiation of the anode line with a nickel filter.

The oxidation kinetics of the nanoparticles of copper in continuous heating and subsequent cooling in air (at a rate of 10°C/min) in the temperature range 20–650°C was investigated using a TGA-7 thermogravimetric analyser.

Experimental results

The investigations of the macrostructure and elemental composition of the transverse sections of the Cu–NaCl condensates showed the uniform distribution of the elements (copper, sodium, chloride, oxygen) in the thickness of the condensate (Fig. 1). This indicates the constant ratio of the rates of evaporation and condensation of the individual components. Examinations of the elemental composition of the condensate with different content of copper in the cross-section showed the presence of oxygen in the amount exceeding the amount required for the stoichiometric composition of copper oxides (Fig. 2). The experimental results show that the ratio of the atomic percent of oxygen and copper (O/Cu) depends on the mass fraction of copper and decreases with the increase of the amount of copper in the condensate (Fig. 2). The high adsorption capacity in respect of oxygen is explained by the presence of small nanoparticles in the condensate.

The small nanoparticles of the metals are characterised by excess energy and high chemical activity [1]. In the condensates, containing 15–30 wt.% of copper, the probability of aggregation of the nanoparticles in the vapour flow and in deposition on the substrate is high, and the ratio of oxygen and copper approaches the stoichiometric ratio (Fig. 2), and this confirms the high adsorption capacity of the small nanoparticles in respect of oxygen [1]. The increase of the substrate temperature T_s in the production of the condensates reduces the ratio of the atomic percent of oxygen and copper (Fig. 2). This is associated mainly with the increase of the

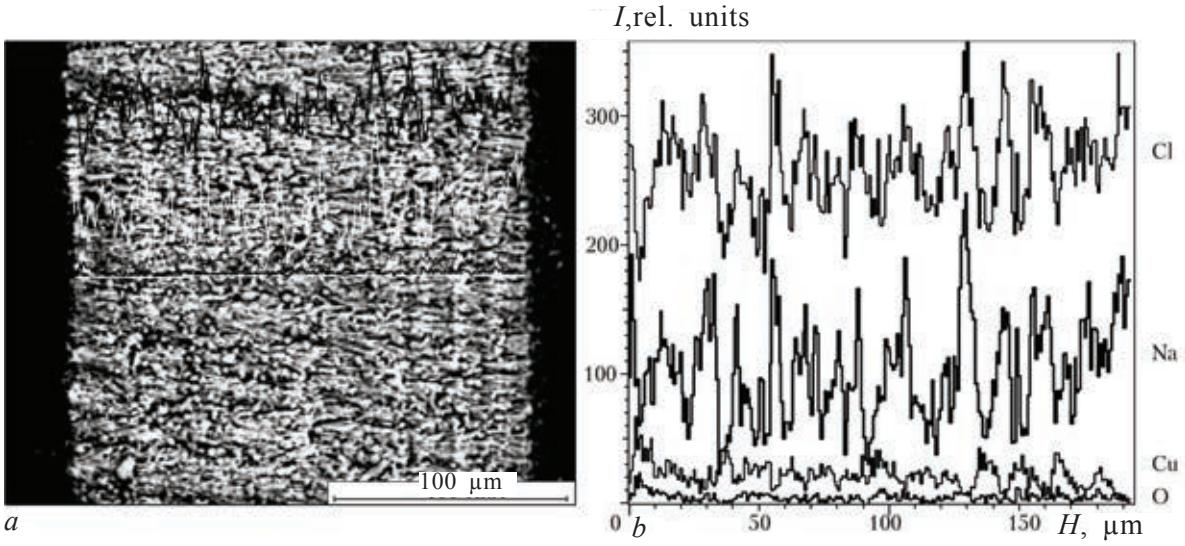

Fig. 1. Microstructure (× 530) of the Cu–NaCl condensate (a) and the distribution of the elements in the thickness of the condensate (b); T_s = 30–50°C; I) intensity, H) the thickness of the condensate.

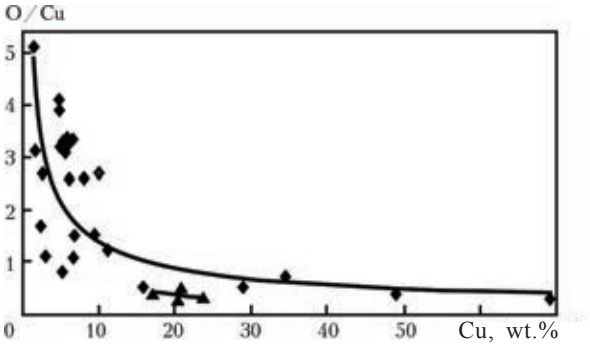

Fig. 2. Dependence of the ratio of the concentration of oxygen and copper (O/Cu) on the copper content of the condensates with the composition Cu–NaCl at T_s, °C: 1) 40–50; 2) 200.

size of the nanoparticles and the reduction of the total surface area of the nanoparticles.

Investigation of the thin cleavage sections of the Cu–NaCl condensates by transmission electron microscopy showed the presence of a nanosized substance (Fig. 3) whose phase composition corresponded mainly to Cu_2O. More information on the phase composition of the nanoparticles in relation to the copper content of the condensate is provided by the results of x-ray diffraction analysis (Table 1).

Analysis of the experimental results shows that at a copper content of the condensate of up to 20 wt.% when the probability of gradation of the nanoparticles in the mixture vapour flow on the deposition on the substrate is small, Cu_2O and CuO (Table 1) form in the porous condensate with the fine nanoparticles in air as confirmed by x-ray phase analysis.

At a mass fraction of copper in the condensate of 20–30%, the probability of aggregation of the nanoparticles in the mixture vapour flow and in deposition decreases. Thus, the condensate contains mainly the Cu_2O phase (Table 1).

At a copper content of 30–15 wt.%, the fraction of the large nanoparticles increases; in addition to the large amount of Cu_2O, the CuO phase and copper were also detected (Table 1). When the copper content of the condensate exceeds 50 wt.%, in addition to the Cu_2O the fraction of the copper phase rapidly increases, and there is no CuO phase (Table 1).

Consequently, physical adsorption of moisture and air by the open surface of the nanoparticles of copper, embedded in the micro- and nanosized pores of the salt matrix, takes place in air. As a result of the atmospheric oxygen, the copper nanoparticles transform to the oxides Cu_2O and CuO (Table 1).

In turn, highly active fine nanoparticles of copper oxide form, interact with the atmospheric oxygen, adsorb moisture and oxygen on their surface, and increase the concentra-

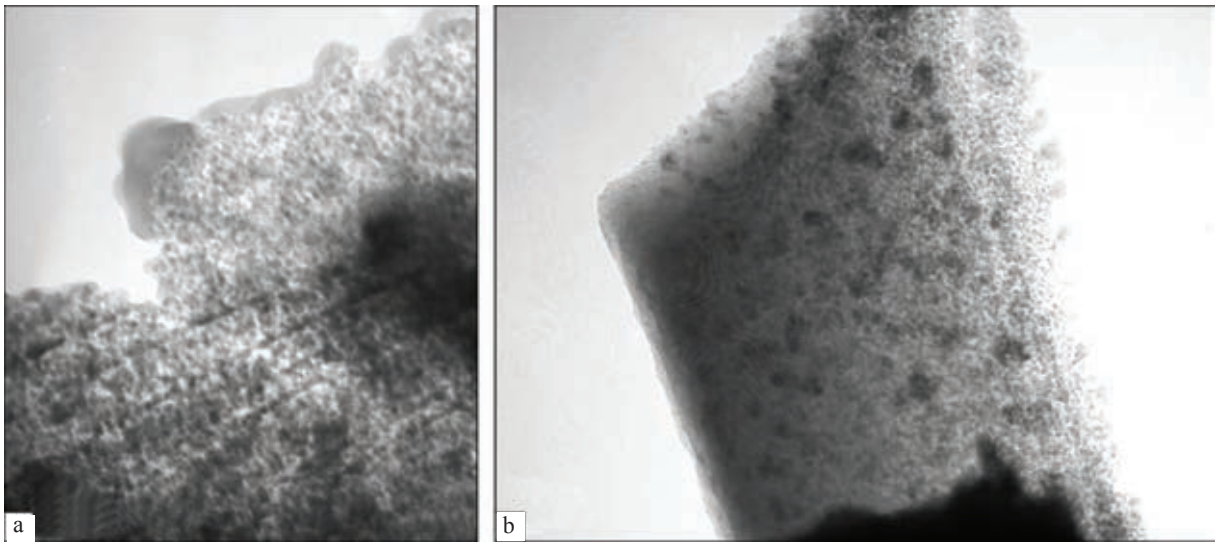

Fig. 3. The microstructure of the initial Cu-Na-Cl condensates; a) × 300,000; b) × 180,000.

Cu–NaCl

No.	Cu_2, wt. %	Phase composition of nanoparticles in Cu-NaCl condensates		
		Cu	Cu_2O	CuO
1	13.7	0	75.0	25.0
2	19.3	0	40.0	60.0
3	23.0	0	100.0	0
4	26.0	0	100.0	0
5	26.0	0	86.2	13.8
6	27.5	0	100.0	0
7	30.0	0	90.9	9.1
8	32.6	13.2	73.6	13.2
9	33.1	13.5	70.3	16.2
10	36.0	0	83.9	16.1
11	47.1	13.9	69.4	16.7
12	55.1	49.1	50.9	0

tion of oxygen in the condensate. This was evident when investigating the elemental composition on the transverse sections of the condensates with a low copper content (Fig. 2, Cu up to 20 wt.%). With increase of the copper concentration in the condensate, the size of the nanoparticles increases, and the activity of the particles decreases. Therefore, the adsorption activity of moist air is lower and, consequently the activity of oxygen also decreases (Fig. 2, Cu >20 wt.%), and this results in the preferential formation of the Cu_2O phase (Table 1, No. 3–7).

With a further increase of the copper concentration and the increase of the size of the nanoparticles, the particles with low activity adsorb almost the same amount of moist air and oxygen (Fig. 2, Cu >20 wt.%). Therefore, the released oxygen (as a result of the formation of pure copper) is partially used for the additional oxidation of Cu_2O to CuO (Table 1, No. 8–11).

In addition to the change in the copper concentration, the phase composition of the nanoparticles in the Cu–NaCl condensates can be regulated by heat treatment of the condensates. Heating in air activates the diffusion processes, leading to coalescence and increase of the size of the nanoparticles and to accelerated oxidation of these particles. This was recorded in thermogravimetric analysis of the kinetics of the relative variation of the mass of the porous Cu–NaCl condensate during heating to a temperature of 650°C, followed by cooling in air.

The investigations carried out on the Cu-NaCl condensates, containing 13.7 wt.% of copper (Fig. 4), show that when the temperature is increased to 400°C (heating at a rate of 10°C/min), the mass of the porous condensate decreases as a result of the removal of moisture (to 100–120°C) and OH-hydroxyl groups (as confirmed by infrared spectroscopy). A further increase of temperature (above 400°C) increases the mass of the porous condensate as a result of the transfer of the Cu_2O phase to the CuO phase (Fig. 4).

After heating to 650°C, the condensate contains only CuO and, therefore, subsequent cooling in heating cycle do not change the face composition of the condensate (Fig. 4). The increase of the annealing time of the condensate in the range of lower temperatures (200–400°C) results in more extensive diffusion processes. Thus, after annealing in air at temperatures of 300 and 400°C for 1 h, the copper is present in the form of the CuO phase in the condensate.

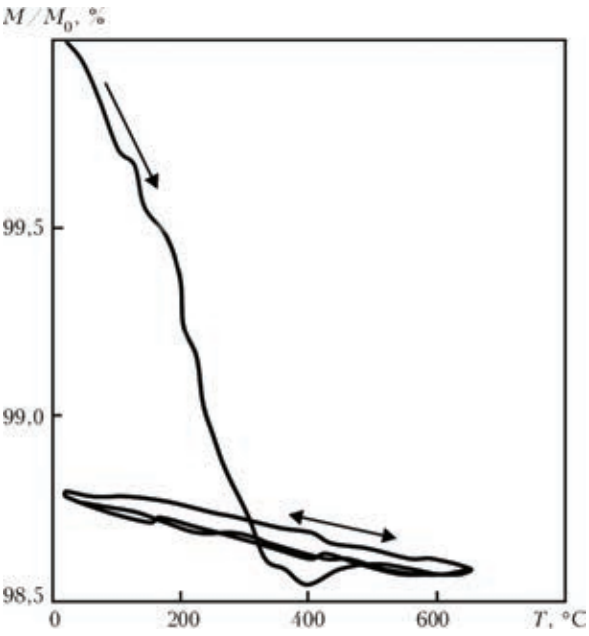

Fig. 4. Kinetics of the relative variation of the mass M of the refined Cu-NaCl condensate (13.7 wt.% of copper) in two cycles of heating and cooling in air; M_0 is the mass of the initial condensate.

When the concentration of copper in the condensate is increased (up to 22 wt.%), the fraction of adsorbed air decreases as a result of the increase of the size of the nanoparticles and the reduction of their activity (Fig. 5, curve 1). To transfer a large amount of Cu_2O phase (Table 1) to the CuO phase, it is necessary to increase the amount of oxygen and, therefore, in heating above 200°C the thermogravimetric analysis curve (TGA) shows an increase of the mass of the specimen of the condensate up to a temperature of 650°C (Fig. 5, curve 1).

After annealing the condensate at 200°C, 10 min, partial diffusion processes, resulting in oxidation and coalescence of the particles, lead to an even larger decrease of the fraction of adsorbed air (Fig. 5, curve 2). The fraction of additional atmospheric oxygen used for the transfer of the Cu2O phase to CuO decreases and this is manifested in a small increase of the mass of the condensate in the second heating cycle (Fig. 5, curve 2). After annealing the condensate for 13 min at 400°C, these parameters are decrease even further (Fig. 5, curve 3).

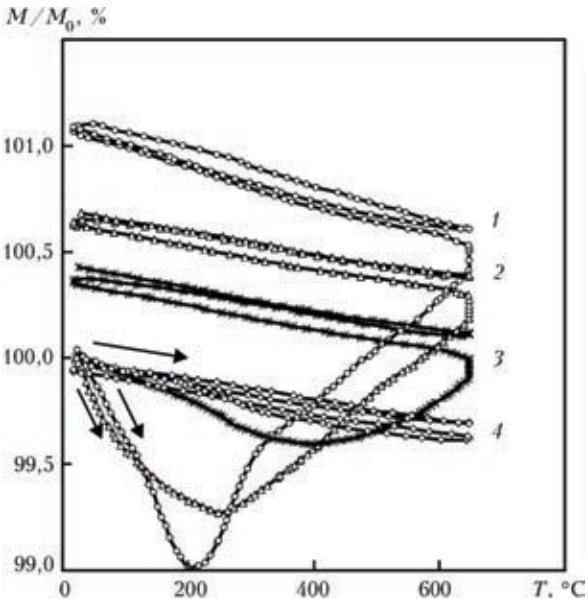

Fig. 5. Kinetics of the relative variation of the mass of the refined Cu-NaCl condensate (22 wt.% of copper) into heating and cooling cycles in air in relation to annealing temperature: 1) initial; 2) 200°C, 10 min; 3) 400°C, 13 min; 4) 650°C, 5 min.

After annealing the condensate at 650°C for 5 min, the diffusion processes which took place resulted in the complete transfer of Cu_2O to CuO, and the enlarged nanoparticles lose their activity to such an extent that the condensate becomes virtually neutral in relation to the sorption properties, and the TGA curves do not show any deviations (Fig. 5, curve 4).

Thus, by controlling the activity (size) of the nanoparticles by means of the copper concentration of the condensate, heating temperature and annealing time, it is possible to produce compositions of the nanomaterials space and copper with the required content of the structural components.

References

1. Serev, G.B., Nanochemistry, Moscow University, Moscow, 2007.
2. Glushchenko, N.N., Physical-chemical relationships of the biological effect of high-dispersion powders of metals, Dissertation, Moscow, 1988.
3. Glushchenko, N.N., et al., Khim. Fizika, 2002, No. 4, 79–85.
4. Chekman, I.S., et al., Mistetstvo likuvaniya, 2008, No. 5, 32–34.
5. Movchan, B.A., Electron beam technology and new materials in medicine - first steps, Visnik Farmakologii i Farmatsii, 2007, No. 12, 5–13.
6. Paton, B.E., et al., Ukrainian Patent 87117, MPC V 82 V3/00.
7. Movchan, B.A., et al., in Proc. Int. Conf. HighMatTech, Kiev, 2007.

Submitted 14.04.2011

Advances in Electrometallurgy 2011 ***9*** *(2) 87–92*
Translated from Sovremennaya Elektrometallurgiya 2011 ***9*** *(2) 26–30*

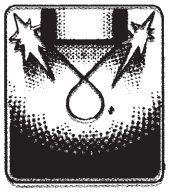

PLASMA ARC TECHNOLOGY

Effect of the displacement of the plasma heat source on the formation of the structure of flat tungsten single crystals

V.A. Shapovalov, V.V. Yakusha, A.N. Gnizdylo, A.P. Smalyukh and D.V. Botvinko

Abstract Methods of layer-by-layer formation of plane single crystals of tungsten in the plasma-induction method of their production are considered. The effect of the nature of movement of the plasma heat source on the formation of the substructure of single crystals was defined. It is shown that using the method of reciprocal movement of molten metal pool the adjustment of deviation of crystallographic axis of growing from the preset direction is possible.

The interest in tungsten single crystals as a structural material, capable of working in special conditions, has been more or less constant over many years. The practical application of tungsten single crystals depends, on the one side, on the extensive examination of the properties of the crystals and improvement of the methods of production of these crystals and, on the other hand, on the development of new high technology equipment.

Large profiled single crystals of refractory metals, produced at the E.O. Paton Electric Welding Institute, Kiev, are regarded as 'ahead of their time'. Their potential has not as yet been completely specified. In particular, at a conference concerned with plasma physics and controlled thermonuclear synthesis, it has been noted that in the realisation of the project of the International Experimental Thermonuclear Reactor, it is very important to investigate the possibilities of using tungsten in equipment with the possible complete a replacement of all materials facing the plasma by tungsten [1–4]. Recently, special attention has been paid to the processes of production of large single crystals of aluminium nitride (AlN) for the production of ultraviolet light diodes (UV LEDs). One of the possible materials for crucibles for growing these crystals is tungsten [5,6]. The application for these purposes of single crystal tungsten eliminates the shortcomings of polycrystalline tungsten associated with its porosity, brittleness and corrosion resistance.

The effective application of large profiled tungsten single crystals depends on the improvement of the method of production and of quality. The aim of the present investigation is to determine the effect of the nature of movement of the local pool of liquid metal on the properties of the substructure of the produced single crystals.

The profiled single crystals of refractory metals in the form of sheets, tubular components or other shapes are produced by layer growth. The simplest method of formation of the moving zone is associated with the application of a moving heat source. Feeding the metal pool, moving along a specific trajectory, it is possible to grow single crystal components. Depending on the profile of the future crystal, the displacement trajectory of the metal pool maybe organised by one of the following three variants: along a spiral, translational, successive.

The process of plasma induction growth of flat single crystals of refractory metals [7] the plasma heat source scans the surface of the crystal being grown, moving the liquid metal pool from one final position to another one. Rod material is fed into the metal pool by droplet transfer. Consequently, the direction of movement of the solidification front is predetermined by the direction of movement of the plasma torch.

The solidification theory shows that additional arrangement of the atoms of the crystal lattice (formation of the single crystal) takes place in the direction of normals to the surface of the solidification front [8–10]. Consequently, the properties of the substructure of the single crystals depend on the nature of movement of the plasma source, i.e., on the algorithm of displacement of the liquid metal pool.

In plasma induction growth of flat single crystal billets it is recommended to use the second or third variant (Fig. 1). The limiting thickness of the grown layer at the edge of the given width is determined by the maximum volume of the liquid pool, capable of stable (without spilling) movement in the specific thermal and rate conditions.

The seat crystal was in the form of a tungsten single crystal produced by plasma induction zone melting with the size of 5 × 20 × 50 mm. The growth process was realised in UP-122 equipment.

The consumable material was in the form of bars of pure tungsten, grade VCh, diameter 8 mm. The plasma forming gas was a mixture consisting of 70% helium and 30% argon. In the growth process, the speed of the plasma source was 14 mm/min. The plasma torch current was varied in the range 380–400 A, arc voltage was 38–40 V. The power of additional induction heating was maintained at the level of 0.4 of the nominal value.

The process of growth consisted of the following operations. After preheating the seed

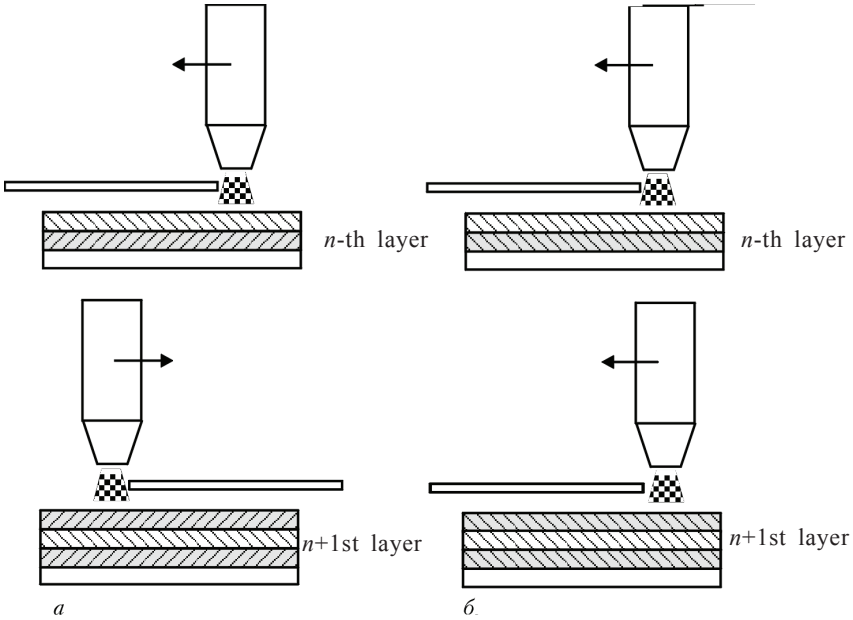

Fig. 1. Algorithm of movement of the liquid metal pool: a) translational movement; b) movement in one side.

in an induction coil to 1700°C and producing a liquid metal pool using the plasma torch in one of the outer positions, the consumable rod was fed into the zone of the plasma arc and the movement of the plasma torch was activated.

When the liquid metal pool reached the opposite edge of the single crystal, the plasma heat source was switched off and brought into the initial position.

This was followed by the generation of the arc, a pool was produced and a bar was fed into the melting zone. The process was then repeated. Thus, 95 × 20 × 50 mm tungsten single crystals were grown and used for producing sections for metallographic and x-ray diffraction analysis.

In the practice of plasma induction growth of flat single crystals, the thickness of the grown layer is determined by the diameter of the consumable bias determined by the organisation of the technological operation of layer growth in which the consumable bar in movement of the plasma torch from one final position to another remains stationary.

The mass of the grown the metal in a single pass of the plasma torch is approximately equal to the mass of the melted bar with the length equal to the length of the single crystal.

When using the bars with a diameter of 8 mm, the thickness of the growing layer on the face 20–25 mm wide was 2–3 mm. The boundaries between the individual layers can be clearly seen in growth of the single crystals by the method of alternative melting of the bars from one and then the other side.

The etched structure of growth of the cross-section is visible in the form of alternating matt and shiny layers. In the rough approximation, the boundary between the layers shows the contour of the solidification front, included in the given section (Fig. 2).

In [11] it was reported that the alternating layers are characterised by a small (less than 1 min) misorientation in relation to each

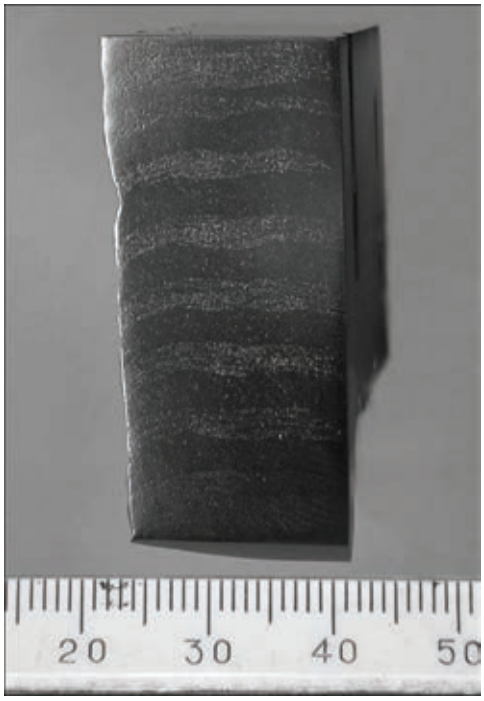

Fig. 2. Microstructure of the cross-section of tungsten single crystals (110).

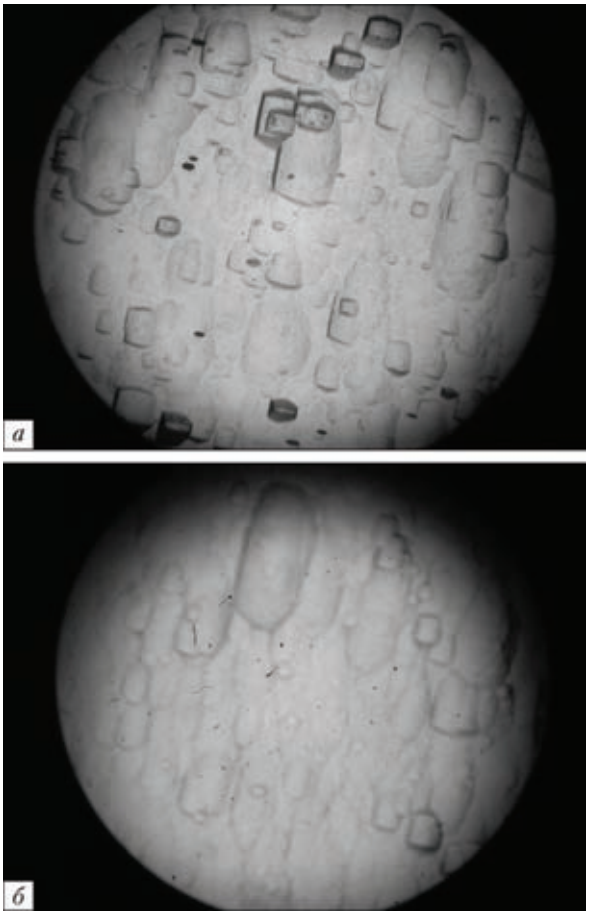

Fig. 3. Structure (× 250) of the growth of a flat tungsten single crystal: a) matt; b) shiny layer.

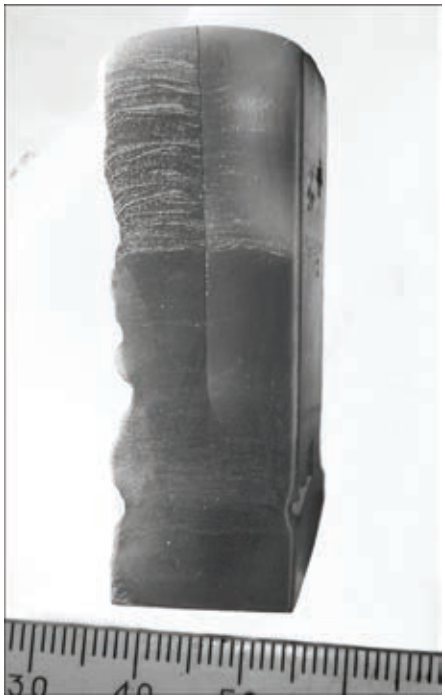

Fig. 4. Microstructure of the cross-section of a tungsten single crystal (110).

other, reflected in different etching capacity of the layers grown on different sides. The structure of growth of the matt layers was characterised by a more pronounced relief and consisted of multifaceted projections, and the shiny layers consisted of the elongated projections of the oval form (Fig. 3).

The structure of the growth of the single crystals, produced by growth in one direction, does not show any alternating matt and shiny bands (Fig. 4). The shape of the contour of the solidification front is also visible and has the form identical with the first variant.

The macrostructure of the investigated single crystal in the cross-section consists of two large blocks with a sharp interface. The 'coarse' boundary appears at the 17 mm horizon and confirms the assumption on the existence of an incubation period in the development of the banded structure. The boundary divides the body of the crystal into two equal parts and extends along the axis of growth.

The evolution of the growth structure in the cross-section of the crystal provides objective information on the large misorientation

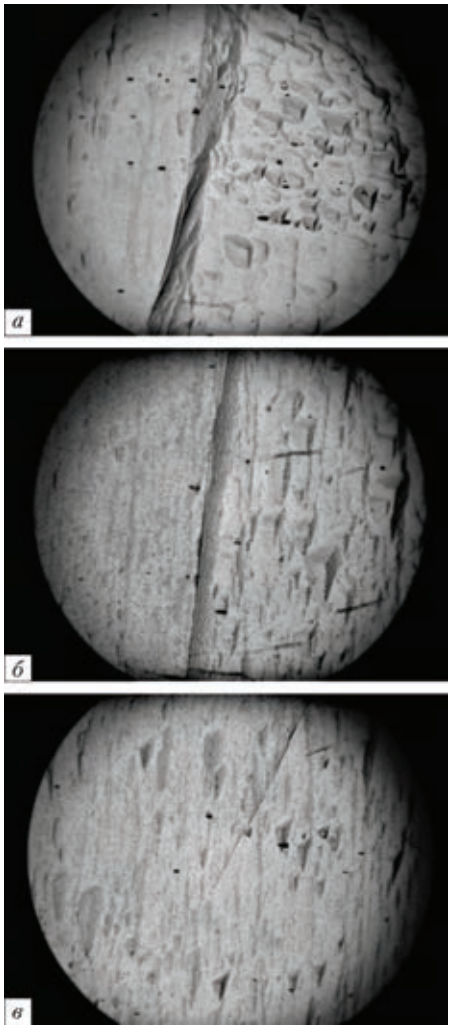

Fig. 5. Evolution of the structure (× 250) of growth in the horizon 50 (a), 30 (b) and 17 (c) mm.

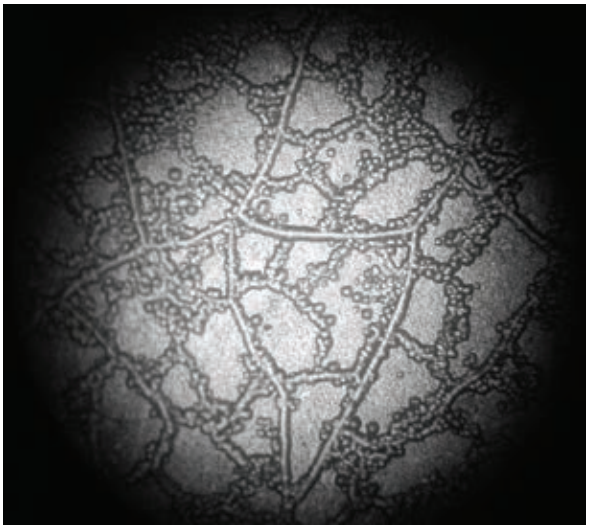

Fig. 6. Dislocation structure (× 250) of a flat tungsten single crystal (100.

angle of the adjacent subgrains (Fig. 5). The absolute difference in the structure of growth in the upper part of the billet indicates the formation of a bicrystal.

The controlling factor of formation of the effect crystals are the thermal conditions of crystallisation which have a strong effect not only on the density of the dislocations in the crystals but also on the concentration of other defects of the crystal structure which are a consequence of plastic deformation of the crystals in the field of thermal stresses.

The dislocation structure of the crystal (Fig. 6) consists of rows of dislocations, forming the boundaries of the subgrains of the second order which contain both the individual dislocations and their groups, forming substructures with a lower order.

As a result of switching on and switching off the plasma arc on both sides of the billet, the crystal is subjected to cyclic thermal shocks, repeated from layer to layer. In the process of growth and cooling of the crystal, the temperature difference in the surface of the grown phase and the surface of the seed crystal plays an important role in the formation of thermal stresses in the crystal. The stresses buildup and the relaxation of thermal stresses results in the formation of a coarse structure.

The experimental results show that thermal cycling, taking place during growth by the method of translational displacement of the plasma torch does not cause any significant disturbances in the formation of the structure (Fig. 7).

X-ray topographs of the longitudinal section show the characteristic banded structure with small inclined intermittent boundaries. The bands are extended along the growth axis. The structure of the seed is inherited by the single crystal and the inclined boundaries of the crystal are straightened during growth.

The diffraction pattern of the structural element in the cross-section normal to the girls direction (Fig. 8) shows the presence of a fragmented section in the centre with the boundary dividing the investigated plane into two approximately equal parts. In all likelihood, this is associated with the given the symmetry of heating in the field of the induction coil. A more fragmented structure is detected in the surface side layer. The misorientation within the specimen does not exceed 5°.

Thus, the application of the method of

Fig. 7. X-ray topograph of the longitudinal section of a flat tungsten single crystal (110).

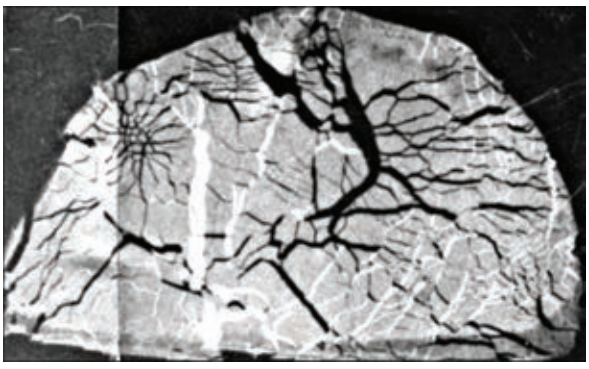

Fig. 8. X-ray topographs of the cross-section of a flat tungsten single crystal.

translation growth produces single crystal with a more perfect structure in comparison with the growth in one direction only. The thermal conditions of growth are one of the controlling factors for producing perfect crystals.

The unsuitable thermal conditions in gradual growth do not make it possible to produce single crystals of higher quality in comparison with the translational method. The periodic variation of the direction of arrangement eliminates the possible deviations of the given crystallographic axes of the crystal growth and support the growth of high quality single crystals.

References

1. http://www.fpl.gpi.ru/Zvenigorod/XXXVIII/R/ru/QM-Kurnaev.doc.
2. http://www.fpl.gpi.ru/Zvenigorod/XXXVIII/E/ru/PF_Khimchenko.doc.
3. http://www.fpl.gpi.ru/Zvenigorod/XXXVIII/Mu/ru/BF-Khripunov.doc.
4. http://www.fpl.gpi.ru/Zvenigorod/XXXVIII/R/ru/QL-Khimchenko.doc.
5. http://www.crystal-is.com/products.cfm.
6. Juan Li, et al., Chinese J. Struct. Chem., 2007, No. 10, 1203–1207.
7. Zhadkevich, M.L., et al., Probl. Spets. Elektrometall. 2001, No. 4, 27–31.
8. Brenner, S.S., Theory and practice of growth of single crystals, Metallurgiya, Moscow, 1960.
9. Sheftal', N.N. (editor), Processes of growth of single crystals, Metallurgiya, Moscow, 1968.
10. Goodman, K. (editor), The growth of crystals. Theory of growth and method of growing crystals,Mir, Moscow, 1977.
11. Kovalenko, A.A., et al., Probl. Spets. Elektrometall., 1994, No. 1, 63–70.

Submitted 28.4.2011

Advances in Electrometallurgy 2011 ***9*** *(2) 93–95*
Translated from Sovremennaya Elektrometallurgiya 2011 ***9*** *(2) 31–33*

GENERAL PROBLEMS OF METALLURGY

Zone recrystallisation of a cast intermetallic alloy based on TiAl and alloyed with niobium and chromium

G.M. Grigorenko, V.V. Lakomskii, I.I. Statkevich, R.V. Kozin, E.A. Asnis, N.V. Piskun, V.A. Berezos

E.O. Paton Electric Welding Institute, Kiev

Abstract Equipment has been designed and conditions have been developed for induction zonal melting of a cast intermetallic alloy on the Ti-Al base, alloyed with niobium and chromium providing directed crystallization and increased strength and ductility at room temperature.

The intermetallic compounds, including those based on titanium aluminide, are highly promising materials for the manufacture of components and sections in aerospace technology. However, technological treatment and industrial application of these materials are complicated by low plasticity at room temperature – the main shortcoming of these alloys.

At the present time, various measures are taken to increase the plasticity of these materials directed to the development of both new alloys ('ortho'-alloys, niobium content 22–25 wt.%) and methods and techniques of treatment of the available alloys [1,2]. In particular, the methods include thermal and deformation treatment which produces intermetallic compounds with small grain sizes and a specific structure (reduction of the size of the α_2-phase and its more uniform distribution in the body of the grain). All these factors increase the plasticity of low and high temperatures.

The plasticity of titanium aluminides can be increased by alloying with chromium, niobium or other elements, and also by ensuring the directionality of the structure of the metal. Alloying of the γ-aluminide of titanium results in the formation of structural components such as α_2- and 'ortho'-phases, but the required improvement of plasticity is not achieved in this case [2,3].

The experimental results also show that the directional structure increases the plastic properties of the metal [2,3]. The directional structure can be reduced as a result of, for example, zone recrystallisation. Zone crystallisation, similar to zone melting [4], ensures

the directionality of the secondary grains and this improves the plasticity without changing the strength at both low and elevated temperatures.

This technology is based on the treatment of specimens by some heat source, travelling along the specimen. In this case, it is the effect of the high-frequency electromagnetic field. It is necessary to determine only the energy parameters combined with the speed of movement of the heating front.

A very efficient method of influencing the intermetallic compound to increase its plasticity is zone recrystallisation resulting in the directional crystallisation [3]. For the correctly selected technology of melting, the solidification front approaches the planar form. This is accompanied by the more uniform distribution of impurities in the cross-section of the volume of the ingot, and the level of the stress state also decreases. Consequently, the plasticity of the metal is improved.

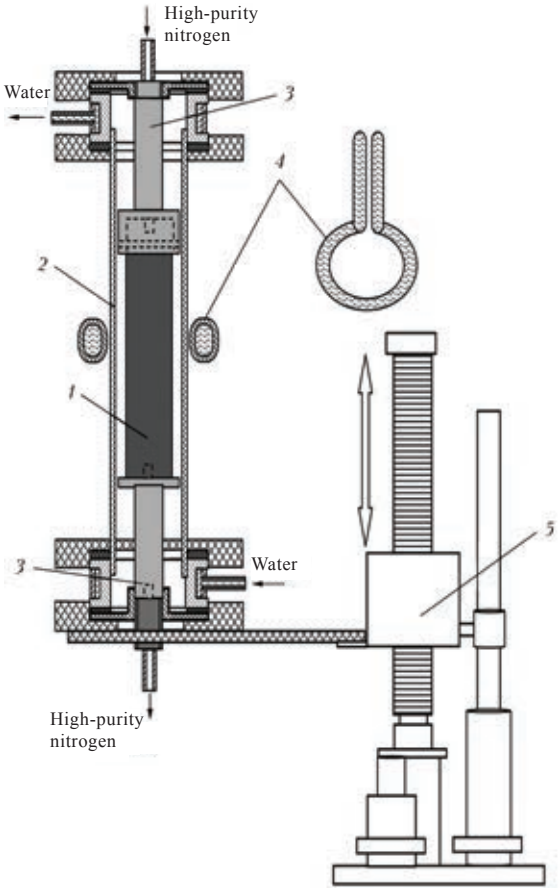

Fig. 1. Diagram of equipment for induction zone melting: 1) remelted specimens; 2) quartz tube; 3) holders of specimens (upper and lower); 4) induction coil; 5) displacement mechanism.

The E.O. Paton Electric Welding Institute, Kiev carried out investigations to develop a technology of induction zone melting of TiAl intermetallic compound. To increase the plasticity of the compound, the material was subjected to recrystallisation.

Special equipment was developed for induction zone melting of the specimens of the intermetallic compound (Fig. 1).

Equipment consists of two main parts: the melting chamber and the mechanism for moving the specimen.

The melting chamber has the form of a quartz tube with a diameter of 20 mm which contains the upper and lower watercooled holders. The holders are used to secure intermetallic specimens with the size of 10 × 10 × 100 mm, produced by electric erosion cutting. High purity argon is passed through the tube during melting in other to protect the molten zone and the heated sections of the specimen. The argon flow rate is controlled with a flowrate metre. The tube together with the specimen is involved along the stationary induction coil using the displacement mechanism providing the speed of movement from 10 to 400 mm/h. The specimens is heated with high-frequency current from the high-frequency generator. The determined energy and speed conditions of zone recrystallisation resulted in flat smooth specimens with a clean shiny surface.

The E.O. Paton Electric Welding Institute, Kiev, used the method of electron beam melting [4] for melting of the intermetallic compound of the TiAl system of the following composition, at.%: Ti–52Al–2Nb–2Cr [5] which was subsequently remelted in the equipment for induction zone melting.

The conditions of induction zone melting were as follows: melting speed 150 mm/h; current 1.7 A; voltage 1.8 kV; frequency 66 kHz.

Investigations of the structure and mechanical characteristics of the specimens after zone recrystallisation show that the selected conditions of zone melting resulted in the

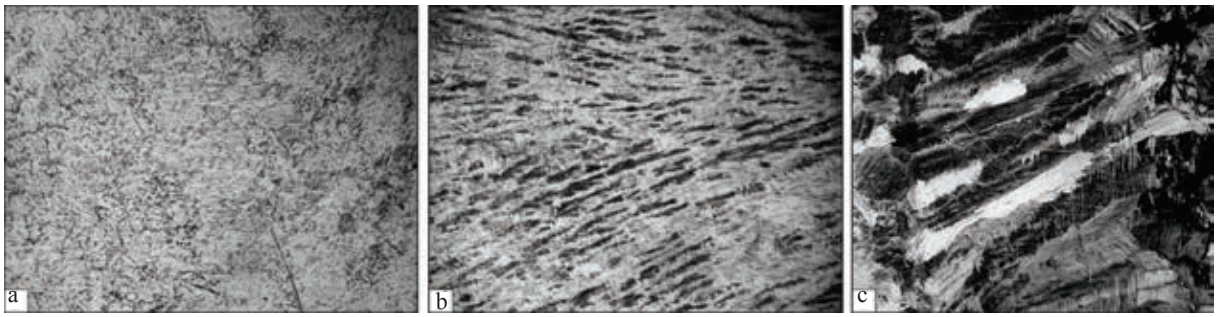

Fig. 2. Microstructure of titanium aluminide after electron beam remelting (a) and zone recrystallisation (b, c); a, b) × 25; c) ×200.

directional crystallisation of the ingot (Fig. 2b, c). For comparison, Fig. 2a shows the microstructure of the intermetallic compound after electron beam melting with an intermediate container (cold hearth). The microstructure shows large grains with lamellae, representing the α_2-phase, distributed in them under different crystallographic directions. In addition, there were small light areas of the β-phase determined by the addition to the alloy of niobium which is an β-stabiliser. The fracture surfaces of the specimens show that the fraction of the ductile component increased. The results of the bend tests on the specimens indicate that the bend angle can reach 30° at room and elevated temperatures (up to 800°C).

The results of the tensile tests carried out in the room temperature shows that the strength of the intermetallic compound after zone melting equals 580 MPa, the relative elongation 2.2%, whereas the ultimate strength of the parent (remelted) intermetallic compound equals 524 MPa, relative elongation 0.8%.

Thus, the method of zone recrystallisation, based on the application of the high-frequency electromagnetic field, results in the directional structure of titanium aluminide and, consequently, improves the plasticity properties of this material without reducing the strength characteristics.

References

1. Povarova, K.B. and Bannykh, O.A., Materialovedenie, 1999, No. 2, 27–32
2. Kuznetsov, .V., et al., Metally, 2002, No. 6, 102–110.
3. Pfann, W., Zone melting, Mir, Moscow, 1970.
4. Paton, B.E., et al., Electron beam melting of refractory and high-reactivity metals, Naukova Dumka, Kiev, 2008.
5. Zhuk, G.V., et al., Sovremennaya Elektrometallurgiya, 2003. No. 4, 20-22.

Submitted 24.3.2011

Advances in Electrometallurgy 2011 ***9*** *(2) 96–100*
Translated from Sovremennaya Elektrometallurgiya 2011 ***9*** *(2) 34–37*

Development of melting and furnace treatment of steel using the Designingmelt software

R.V. Sinyakov

Donetsk National Technical University, Donetsk

Abstract: Description of programming software DesigningMelt, designed for the development of technological processes, assessment of application of new types of materials and equipment, is given. Using the DesigningMelt, it is possible to model technological processes, proceeding in most of steel melting units (converter, arc steel melting furnace, furnace-ladle, vacuumator) as well as to create the optimum technological routes of melting and processing of steel.

Introduction

Every year, the requirements on the quality of steel products, industrial flexibility and duration of development of the technology of melting varying grades of steel in concrete production conditions increase. Currently, the solution of tasks is impose on the automated process control system [1–3]. The introduction of such systems can not only effectively control the process, but also increase productivity, improve economic performance and product quality [4, 5].

However, in case of need for the development of steelmaking technology, new brand-specific working conditions, equipment upgrades, evaluate new materials, etc., existing systems do not always have the appropriate tools to solve these problems. This is due, firstly, to the need to attract design apparatus that, with respect to the metallurgical process is complex and requires a significant amount of work, and second – with the use of automated systems of semi-empirical models describing the processes occurring in the steel bath as evidenced by reports of process optimization through the use of automation (they are partial in nature and are within the scope of existing technology).

Problem statement

In this paper, the task is to create a tool with which the technologist can develop and evaluate the process of melting or secondary treatment given of the steel grade, the technological route of processing, as well as determine the impact of modernization equipment for technological and economic indicators.

Basic materials research

In the development of the software package DesigningMelt it was assumed that all the algorithms and calculations of should be based on a rigorous theoretical model, which allows even without statistical binding to solve a wide range of practical problems. Therefore, an approach that is implemented in the program Excalibur was used as the core of the system [6].

The core of the program is based on a thermodynamic model of the condensed phase and the enthalpy heat balance. This allows the calculation of thermodynamic equilibrium in multicomponent heterogeneous metal–slag–gas system; the temperature of the system based on the enthalpy

heat balance; the partial pressures of atomic and molecular constituents of the gas phase, all the integral and partial thermodynamic functions of the components of the system and take into account the heat energy, temperature, and the aggregation state of materials.

The development of new technology included to the project of melting in time, coordination of the modes of the equipment, commissioning, materials, assessment of changes in the basic parameters of heat (chemical composition, mass and temperature of melted products) over time, etc.

Development of the melting project (or processing) with time using the principles of design, presented in [7], and recording of the kinetics of the processes were carried out according to the procedure described in [8].

The proposed software system contains four main modes: the development of a new melt; a continuous technological process, ing-through process creation, processing of previous melts and development on their basis of optimal melting.

Developing a new process begins with a description of the metallurgical unit (Fig. 1 a) and the structure of the process (Fig. 1 b) through the dialog windows.

The description of the unit includes details such as capacity, weight of the lining, full and working volumes. The structure of the process is a sequence of periods melting of a certain duration. For example, for an electric arc furnace with one charge and one discharge the number of periods will be five (Fig. 1b). Most of the periods are contained in the database of the programs and the technologist can selected the required one, specify its duration and start time.

Next, the steelmaking unit is equipped with the necessary equipment for conducting melting (Fig. 2). Quite a large selection of equipment of modern steel-making units is presented in the program database. If the required equipment not available in the list, similar one should be selected. In the future, this equipment can be edited and already stored in the database for future use. To edit the many options available, as should be made the main type of material used, technical and technological constraints on the input mode of the material.

After doing all these procedures become the main form of melting of the project (Figure 3) with the average mode (time moments, cost) input materials and energy. Above shows the preliminary information about the trajectory of the process (temperature, mass of metal and slag, slag and gas produced, basic slag).

Here it is possible to design the process - to change modes input materials, temporary moments of return of materials (I scrap), the duration of individual periods and the entire heat, and add or delete material as well as add, delete and edit the equipment used. The end of a process is an imitation of heat cre-

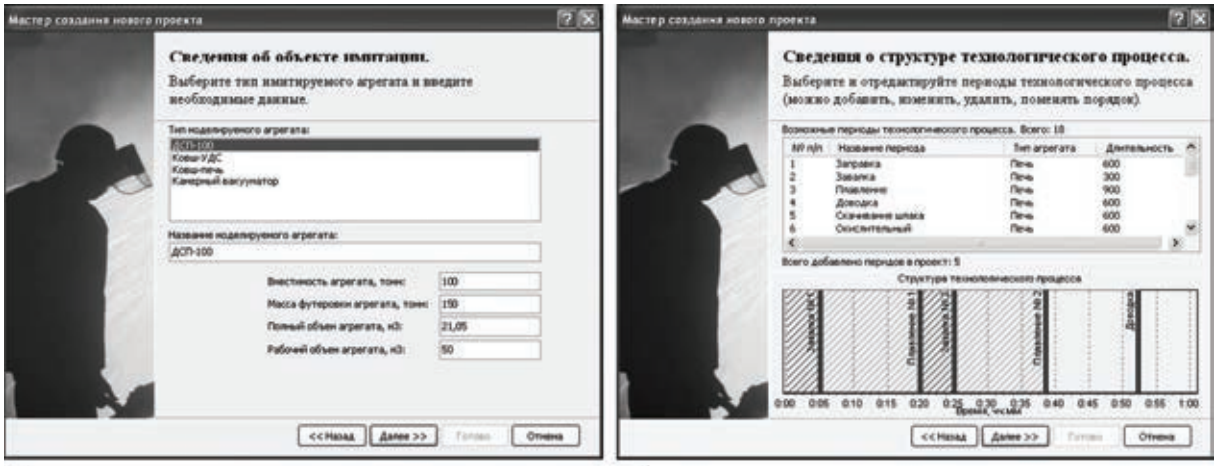

а *б*

Fig. 1. Description of the metallurgical aggregate (a) and structure of the process (b).

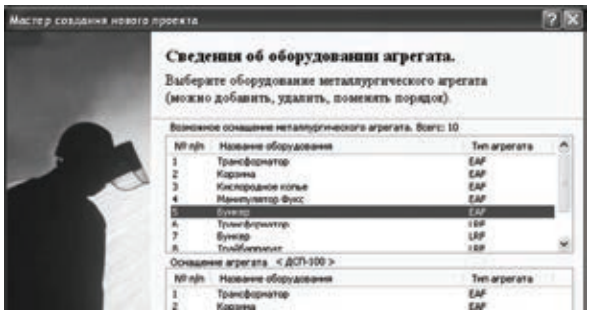

Fig. 2. Steelmelting E=equipment.

ated under the project.

For given levels of input materials and energy, taking into account the full material and energy balances, thermodynamic calculations and kinetic correction (flow rate of reagents, dissolution rate averaging bath on the chemical composition and temperature), simulated with a predetermined melting (relatively small) time step .

After the calculation operator (technologist) and the final details of the trajectory of the process (Fig. 4a, b).

In addition to these parameters, you can see changes in the chemical composition of the metal and slag during melting, the composition of released gases, as well as material and heat balances of the process.

If necessary, the operator (technologist) could return to the main form (Fig. 3), make any changes in the draft and re-run simulations melting, to assess not only the calculated melting technology, but also to compare it with previous version. These results can be

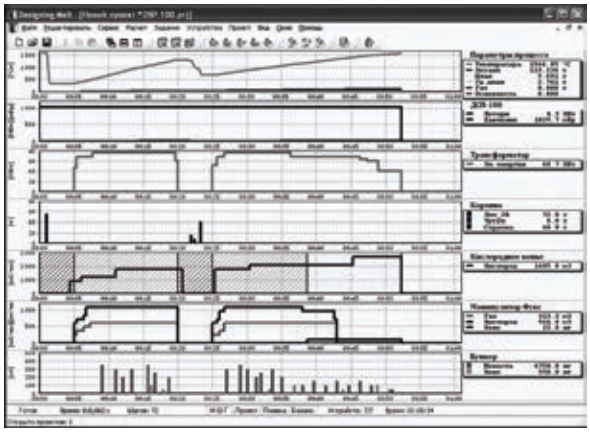

Fig. 3. The main form of the DesigningMelt software.

any number. Of these, the best choice.

Optimization criterion can be re-distribution of costs and the duration of melting, the time of release, the coordination with adjacent redistributions, etc. This includes the introduction of new and upgrade existing equipment, replacement of one by other, move some operations out of the furnace to furnace processing, assessing the feasibility of new materials, determining the optimal time and the number podvalok, slag regime change, etc.

All results are stored in a database for later analysis or use in the design-through process.

Cross-cutting process is a temporal sequence of operations smelting and processing of steel, in other words, the technological route. For the development and evaluation of a technological route first opened previously established projects, such as smelting in electric arc furnace, alloying and processing production, processing and ladle-furnace vacuum treatment of metal (Fig. 4c).

With the appropriate menu item of the main form opens the form of through rendering TP (Fig. 5). At the top of the table displays the available TA projects with the following information: file name of the project, expanded the project name, type of unit to which the draft. Of open source projects provide possible scenarios of smelting and steel processing, perform simulation. At the end of the scripting calculation results are stored in a file or files for further consideration.

For analysis and correction of existing technology in the program the opportunity I held a retrospective of information on melting (processing) on the main form of the program. Special module allows you to convert the information on past trunks and display it in the form of a project that will analyze, edit and simulate the process.

Batch simulation array of heats, followed by retrospective analysis of the results to create a rational (close to optimal in terms of specific production) technology of smelting and processing of certain grades of steel. With this approach are evaluated not only integrated performance of the process, but also

Fig. 4. View of the form with information about the results of simulation of the melting process (processing) (a), the thermal and material imbalance of melting (processing) (b), and available projects for melting and processing of steel (c).

time, place and mode of input materials and energy, the composition and mass produced metal and slag, and the temperature of the system at every stage of melting.

Findings

1. Software complex «DesigningMelt» represents a synthesis of recent advances in theory and practice of steel production, assembled in a compact, user-friendly software product intuitive interface.

Fig. 5. The form for calculating the course of the technological process.

2. The presence of a deterministic approach to building software system allows to simulate most of the existing steel-making units (converter, electric arc furnace, ladle furnace, degasser), considering them both individually and as a single processing facility.

3. In addition to solving specific problems - the calculation of the amount of material (charge, deoxidizers, alloying, slag) needed for a given chemical composition of the metal, the calculation of the required cost of energy to melt, - «DesigningMelt» is a tool that allows technologist can develop new processes, evaluate the application of new materials, equipment, and create the optimal technological Routes of smelting and processing of steel. Possible to perform analysis of the problem batches in order to identify their causes and ways to removing them.

4. Using «DesigningMelt» in the development of new technology makes it possible to increase productivity, work quality and reduce errors in the design of the technologist, as well as significantly reduce the development time for the TA.

5. Presented software package can be used in the learning process, allowing students to feel like steel makers, while having the opportunity to make mistakes.

References

1. Ponomarenko A.G., et al., in : Proc. 5th Steelmelt-

ing Congress, Chermetinformatsiya, Moscow, 1999, 174–177
2. Klerichi, P., et al., Metallurg. Pr-vo Tekhnol., 2009, No. 1, 6-9.
3. Nachleger, S., et al., Chernye Metally, 2009, No. 10, 37–43.
4. Martynov, R.N., et al., Elektrometallurgiya, 2002 No. 6, 36–40.
5. Sinyakov, R.N., et al., Metall i lit'e Ukrainy, 2005, No. 3-4, 98-100.
6. Kharchenko, A.V., et at., Sb. tr. DonNTU, 2005, No. 102, 82–91.
7. Sinyakov, R.V., et al., Metall i lit'e Ukrainy, 2001, No. 10-11, 38–44.
8. Ponomarenko, A.G., et al., Vestnik YuUrGU, 2002, No. 2, 32–35.

DonNTU, Donetsk

Advances in Electrometallurgy 2011 ***9*** *(2) 101–108*
Translated from Sovremennaya Elektrometallurgiya 2011 ***9*** *(2) 44–49*

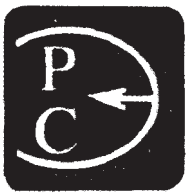

ENERGY SAVING

Computer modelling of thermal and electric processes in an electric calcinator

V.I. Lakomskii, A.M. Pal'ti and D.D. Yurchenko

E.O. Paton Electric Welding Institute, Kiev; Kiev Polytechnical Institute, KADFEM CIC, Kiev

The present work is devoted to the modelLing of heat and electric fields in electric calcinators. Using ANSYS package, the computer analysis of two designs of electric calcinators was made: with and without a throttle. Comparative analysis was made and the higher efficiency of design with the throttle choke was shown. Recommendations are given on its further updating.

In [1], the authors carried out computer modelling of the thermal and electrical fields in electroslag surfacing using a package of applied programs ANSYS. The current work is concerned with similar modelling of the thermal and electrical fields in electric calcinators with [2] and with [3] the throttle.

The electric calcinator is an electrical resistance furnace. The vertical shaft of the furnace is lined with fireclay bricks anda mullite ceiling. The upper graphitized and lower self-baking electrodes are positioned along the axis of the shaft. Anthracite with high electrical resistance is loaded into the furnace. During heating of the anthracite with sublimation gases of coal, the electrical resistance of the anthracite decreases and electric current starts to pass through it. The main heat input into the outer side is provided during electric heating. Baking ensures low specific electrical resistance and mechanical strength at high temperatures which is essential for the cathode lining of aluminium electrolyser.

The aim of the investigations was to study the fields of temperatures and heat flow, the distribution of the electrical potential and current density in the working space of equipment. Two variants of the supplied power were investigated. As in [1], the temperature dependences of the thermal and electrical characteristics of the materials of the investigated object were taken into account. In the process of verification of the model, some of the characteristics of the materials were selected by solving the inverse problems on the basis of the available experimental data on temperature in equipment. Numerical modelling of the thermal and electrical fields was carried out in the same package of applied programs ANSYS.

Formulation of the problem

The physical and geometrical characteristics of the models are presented. The geometry of the models for the case with and without the

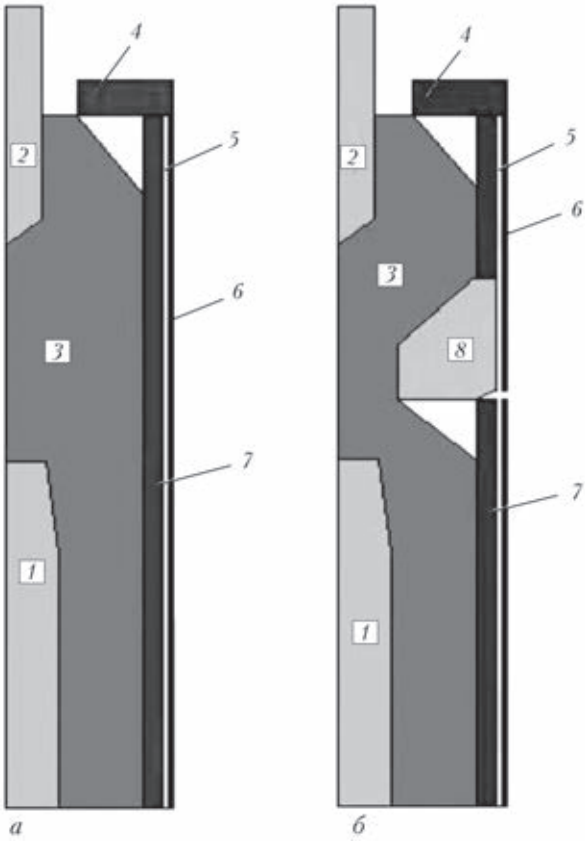

Fig. 1. Geometry of the model without (a) and with the throttle (b).

choke coil is shown in Fig. 1. The legions of solution in both variants include the lower 1 and upper 2 electrodes, the technological space, filled with the anthracite 3, the upper chite made of concrete or fireclay 4, the lining of the shaft of the electric calcinator using fireclay breaks 7, the steel shell 6, the interlayer of mullite insulation 5, and the choke coil 8. The overall dimensions of equipment were as follows: d_{max} = 2.3 m (the diameter of the object); h_{max} = 6.6 m (its height).

The two-dimensional stationary thermal state of the processing was investigated taking into account the effective (convective and radiant) heat exchange of the outer surfaces into the environment with the temperature of 293 K and the removal of heat by water with the same temperature from the lower electrode. The object is characterised by axial symmetry and, consequently, the two-dimensional model in the cylindrical coordinate circuit is investigated. The model takes into account the dependence of the thermophysical characteristics of the thermal anthracite on temperature and the coordinate along the height of the shaft of the furnace.

Slow displacement of the baked material in the furnace shaft at a speed of approximately 0.2–0.3 mm/s determines the stationary nature of the problem. The process is described by a system of equations of stationary heat conductivity and electrical potential. The nonuniform finite-element grids of the investigated object for the case of two geometries were investigated.

The processes in the furnace are described by the equation of stationary heat conductivity with the internal heat sources:

$$\nabla\left(\hat{\lambda}\nabla T\right)+\rho(T)|\mathbf{j}|^2=0, \quad (1)$$

where $T = T(r,z)$ is the temperature field (r and z are the variables of the cylindrical coordinate system); $\lambda(z, r, T)$ is the effective heat conductivity of the region (tensor), W/(m · K); $\rho(T)$ is the specific electrical resistance of thermal anthracite, ohm · m; $\mathbf{j}$ is the vector of current density, A/m^2.

In the cylindrical coordinate system, the equation of nonlinear heat conductivity for the object investigated here has the form

$$\frac{1\partial}{r\partial}\left(r\lambda(z,T)\frac{\partial T}{\partial r}\right)+\frac{\partial}{\partial z}\left(\lambda(z,t)\frac{\partial T}{\partial z}\right)+\rho(\nabla\varphi)^2=0. \quad (2)$$

The electrical field in the object is described by the Laplace equation for the potential

$$\nabla\mathbf{j} = 0 \text{ or } \Delta\varphi = 0, \quad (3)$$

where $\varphi(r,z)$ is the field of the electrical potential.

Everywhere, with the exception of the current supply areas, the current density j_n (or $-\nabla\varphi$), normal to the boundary, is accepted equal to 0.

The conjugate electric thermal problem is investigated, i.e., the thermal and electrical contacts of different areas (lining of the charge, the baked thermal anthracite and the material of the upper and lower electrodes)

are taken into account. The conditions of continuity of temperature and electrical potential are accepted at the boundaries of the regions. The convective heat exchange in the region of the furnace shaft is described by the effective heat conductivity coefficient. The conditions of convective and radiant heat exchange were specified at the boundaries of the regions:

$$-\lambda\frac{\partial T}{\partial r}\bigg|_r = \alpha\left(T - T_o\right) \text{ and } -\lambda\frac{\partial T}{\partial r}\bigg|_r = \sigma\varepsilon_{12}\left(T^4 - T_o^4\right), \quad (4)$$

where the symbol $|_r$ indicates the values of the function at the boundary of the region; T_o is the temperature of the cooling water, air or the walls; σ is the Stefan–Boltzmann constant; ε_{12} is the relative density of the radiating surfaces.

The mathematical models (1)–(4) were presented for all the individual areas of the solution range. The differences in the physical properties of the regions were taken into account by the dependence of the coefficients ρ, λ on the coordinates. The data on the thermophysical characteristics of materials were used [4, 5].

Assumptions of the model and tabulated data

Taking into account the quasi-stationary nature of the process, investigations were carried out into the determination of the state of the space of the shaft with anthracite, corresponding to the available experimental data. The surface of the furnace is in convective and radiant heat exchange with the environment. Air convective heat exchange of the upper electrode and the area of unloading the finished product with the environment takes place. In the region of the supply of current to the upper and lower electrodes there is convective heat exchange with the cooling water. The coefficients of convective heat exchange were selected from the range 10…50 W/(m·K) using the solution of the inverse heat conductivity problems.

The removal of heat by the gases during baking and also by the completed product is determined by integral heat generation (in the present case, by the reduction of the difference of the potentials at the electrodes).

We accept the thermophysical characteristics for the lower electrode and the choke coil: specific heat conductivity (T > 473 K), λ = 7…10 W/(m·K), and electrical resistance ρ = (50…75) μohm·m. The specific heat conductivity of thermal anthracite is approximated by the following linear dependence 373…1173 = (0.41…0.84) W/(m·K). The specific electrical resistance is ρ: = 0.01(1–0.0003t) ohm·m. The density of bulk anthracite with the fraction composition 6…25 mm is 1 t/m^3.

Numerical analysis of temperature and electrical fields

As shown by the investigations of the temperature and pressure of contact resistance of thermal anthracite [6], the contact resistance decreases with increase of these parameters during the movement of thermal anthracite along the furnace shaft. Therefore, in the furnace in which the 'raw' anthracite is subjected to heat treatment, the electrical resistance is stabilised when some temperature of the coal is reached.

Further, in the process of slow movement of the starting material along the shaft of the electric calcinator, the resistance remains almost completely constant. A similar hysteresis dependence of electrical resistance is required when using a more stricter approach to the solution of the non--stationary problem.

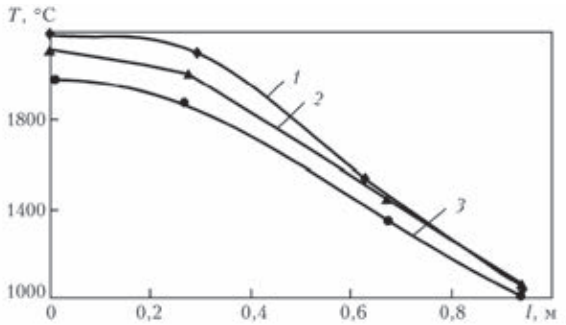

Fig. 2. Temperature distribution in three subsequent horizons in the region between the electrodes (regime I): 1) the first; 2) the second; 3) the third; *l* is the distance from the axis.

We have examined the first approximation to complicated processes in the initial material – the stationary electric thermal model. Therefore, numerical experiments were carried out in which the region of the shaft with anthracite was divided into three zones with each zone having its own temperature dependence of the properties along the height of the furnace (Fig. 2).

In the models, in addition to the nonlinear dependence $\rho(T)$ in a number of zones, there is the anisotropy of the coefficient of heat conductivity of thermal anthracite (along the height and the radius of the furnace shaft) taking into account slow movement of the initial material (stationary approach) and accompanying processes of treatment of the starting material, for example, the interaction of the material with the gases of dry distillation of coal and gases – the products of combustion of coal in the atmosphere of the air sucked into the furnace. Attention is also given to the existence of the additional sources of regeneration, simulating the removal of heat from the furnace with completed thermal anthracite. It should also be mentioned that the approach, which takes into account the phase transition of thermal anthracite to ensure the heat taken away by the material from the furnace, require solving a non-stationary problem.

The sources of heat generation, required for description, are determined as follows. The stationary regime, usually established in the gaps between the acts of sampling completed thermal anthracite, and the heat, taken away from the furnace together with the completed product were taken into account, on the basis of the general reduction of the power supplied to the furnace (working voltage in the furnace).

This voltage will be approximately calculated. It is assumed that the power in the normal technological mode of operation of the furnace is proportional to the yield of the completed product in unit time. As shown by numerical modelling, the evaluation of the potential difference between the electrodes, based on this calculations, is in agreement with experimental values of temperature at the boundaries of the installation (metallic jacket of the furnace). The nature of distribution of the temperature in different horizons of the furnace is in agreement with the state.

Thus, the power of 0.8 MW corresponds to the productivity of 2000 kg/h. The yield of 650 kg/h of thermal anthracite corresponds to these temperatures data. This yield of the product is linked with the following power:

$$(650/2000)\cdot 0.8 = 0.26 \text{ [MW]} \quad (5)$$

The power, taken away from the furnace by completed anthracite is

$$Gc\Delta T/S = (650/3600)1800(800–20)/2.3\approx 0.12 \text{ [MW]} \quad (6)$$

where G is the yield of the completed product, kg/s, c is its heat capacity, J/(kg ·K); ΔT is the superheating of thermal anthracite in relation to the starting (cold) product, K; S is the output cross-section area of the shaft, m^2.

To obtain the required values of the temperature in the model, the basic voltage drop was specified U_1 = 10 V (regime I), and the regime II in which U_2 = 7 V was also simulated.

The spatial division of the grid was car-

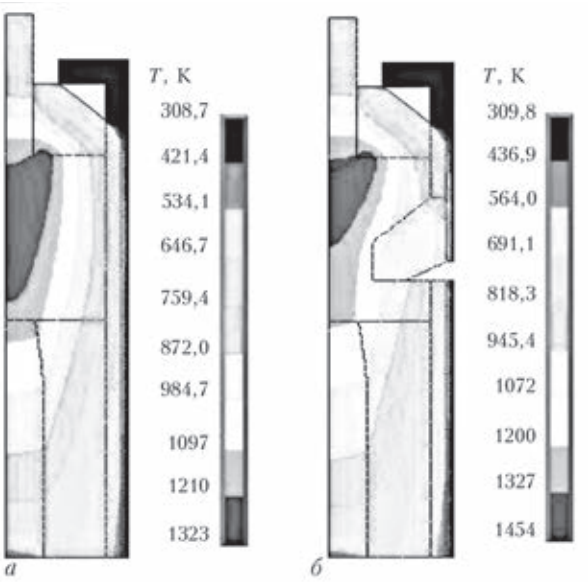

Fig. 3. Total temperature field of the furnace in the regime II (U = 7 V: without the throttle (a), with the throttle (b) (the temperature is given in Kelvins).

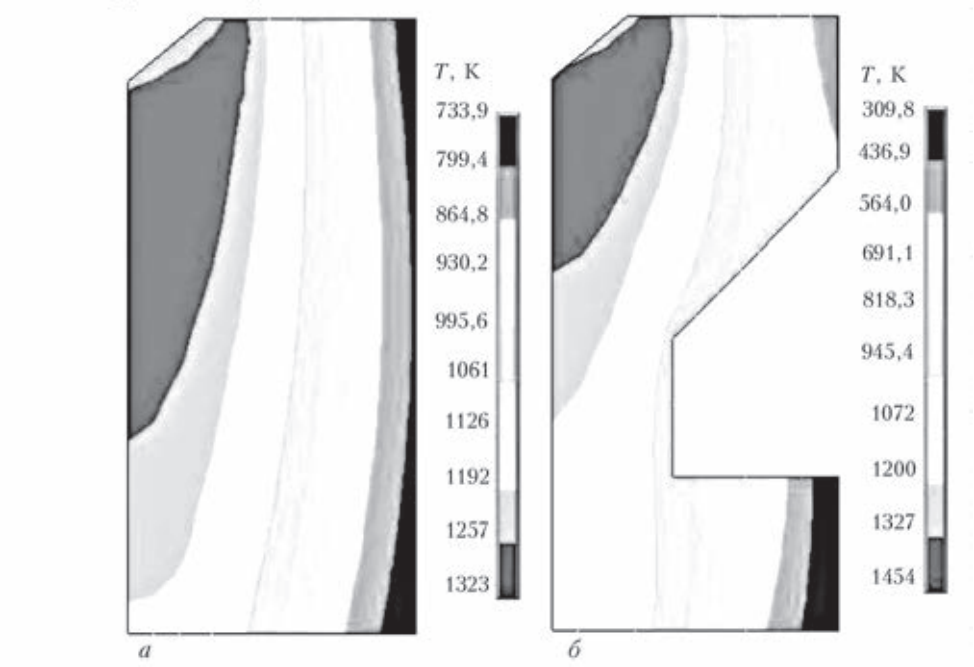

Fig. 4. The temperature field of the section of the furnace shaft (the region below the electrode) in the regime II: a) without the throttle; b) with the throttle.

ried out taking into account the main special features of the structure of the investigated object. This was reflected in the degree of refining of the grid in the individual sections of the shaft space.

Figures 3 and 4 show the total field of distribution of temperature in the furnace and in section for the regime II (the potential difference between the electrodes U = 7 V) in the models with and without the throttle

It is important to note the qualitative nature of the reduced temperature fields and heat flows determined by the absence of accurate data on the actual part the furnace at which the optimum temperatures were recorded at different horizons of the inter-electrodes space and on the outer jacket of equipment. For this reason, the calculated values of temperature in the three horizons are slightly higher than the experimental data (Fig. 2), but the course of variation of these values is approximately the same.

The temperature field shows that the coal is strongly superheated in the inter-electrodes region. More intensive heating at the upper electrode confirms the fact of its more intensive operation in comparison with the lower electrode.

The anisotropy of heat conductivity (along the axis of the furnace shaft it is approximately 30 times higher than in the radial direction) was introduced into the model. The numerical experiments show higher sensitivity of the model to the value of the heat conductivity coefficient along the furnace axis. This is associated with the existence in the real conditions of the longitudinal movement of the mass of anthracite which was taken into account only effectively.

The relatively high heat conductivity along the furnace axis is determined by the presence (in addition to conductive heat exchange) of internal radiant heat exchange between the anthracite particles. Without introducing the anisotropy of the thermal and electrical properties it was not possible to match the experiments with the modelling results.

In the absence of the throttle in the horizontal sections between the electrodes, the temperature values are distributed over a wider range than in the presence of the throttle. Therefore, under the condition that

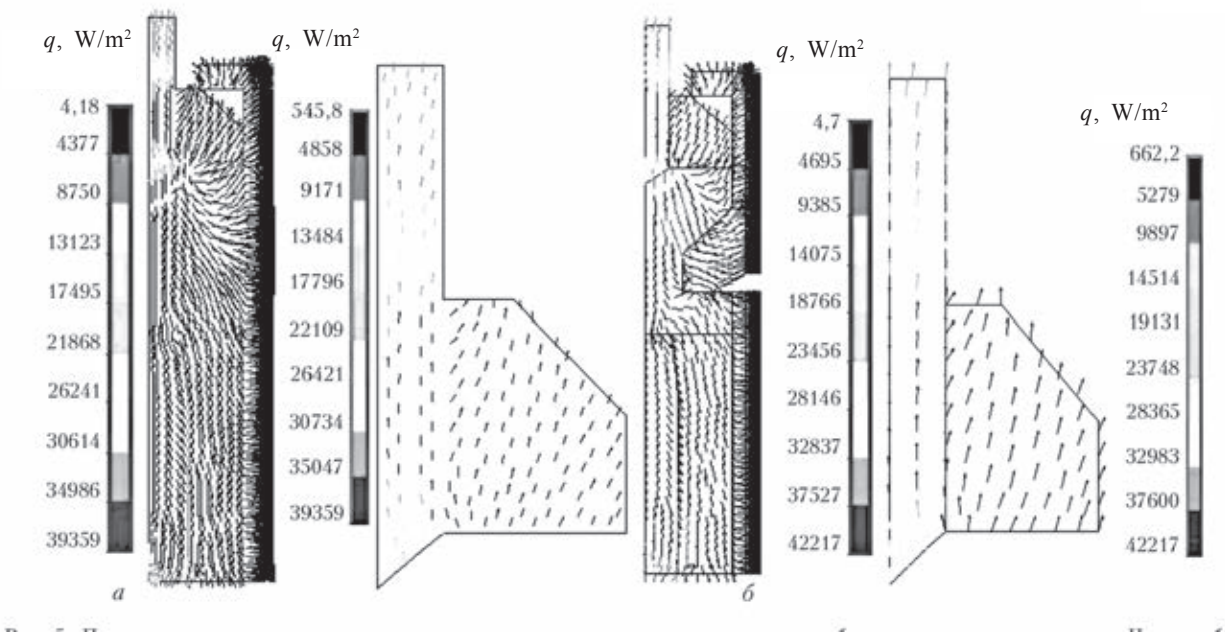

Fig. 5. The field of the vector of the heat flow in the space of the furnace shaft and the section of the field in the vicinity of the electrode in the regime II: a) without the throttle; b) with the throttle.

thermal anthracite reaches the required value of specific electrical resistance in a specific temperature range, then in the absence of the throttle the wider temperature range causes that the mean specific electrical resistance in the horizon of coal at exit from the furnace without the throttle is considerably higher than in its presence.

In the model with the throttle, the temperature range in the horizontal section of the mass of anthracite is smaller than without it and, therefore, the anthracite is processed more uniformly at a higher mean temperature in the horizon.

The temperature range in the gap between the electrodes (regime I) without the throttle is 1233…2593 K, and in the same regime in the model with the throttle it is 1993…2263 K. Baked anthracite has the temperature values in the radial section of the furnace shaft on the level of the middle of the gap between the electrodes. This range can be reduced by changing the design parameters of the throttle and the relative position of the throttle and the electrodes.

We now analyse the distribution of the thermal flows. Figure 5 shows the field of directions of the vector of the heat flow in the space of the furnace and the section of the electrode together with the adjacent region in the regime II.

Comparison of the fields for two different conditions indicate the presence of a large increase of the heat losses through the side jacket of the furnace, and also through the electrodes in the model with a throttle where the losses increased by approximately 10%. The highest values of the heat flow are recorded in the region of the end of the upper electrode (without the throttle 82, with it 90 kW/m^2). The mean value of the flow, moving away from the surface of the furnace jacket, in the regime I with the throttle that not exceed 9.8, without it 9.2 kW/m^2, in the regime II with the throttle 4.5, without it 4.3 kW/m^2.

The level of the heat flows of the upper electrode is an important and readily available parameter for examining the automation of the process. In particular, the high values of the heat flows are obtained in the region of the upper electrode resulting in its more intensive operation.

The main changes in the electrical potential (Fig. 6) take place in the upper sections of the shaft, in the vicinity of the electrode. The presence of the throttle has only a slight

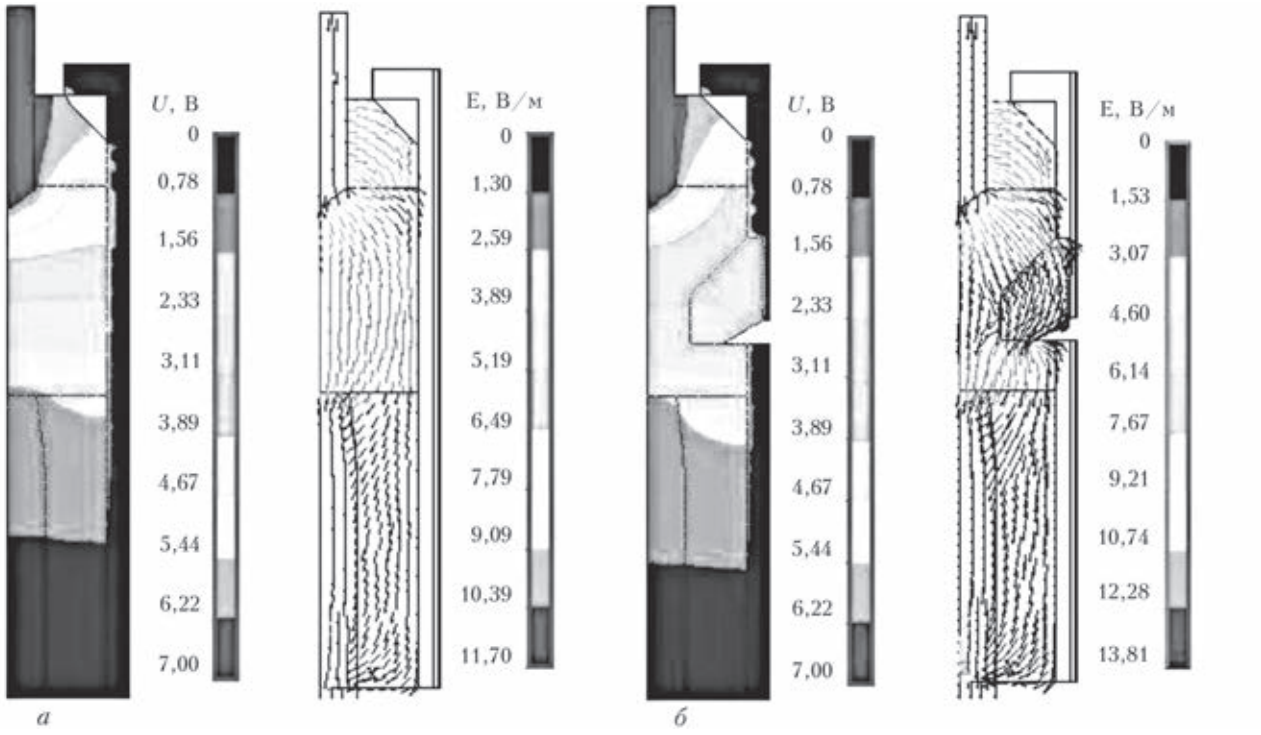

Fig. 6. Distribution of the electrical potential and the strength of the electrical field in the furnace in the regime II: a) without the throttle; b) with the throttle.

effect on their distribution. This is associated with its low specific electrical resistance. At the same time, the most 'dangerous' (from the viewpoint of electrical breakdown) region is situated in the upper part of the furnace. It is assumed that the individual regions of the furnace (the jacket, throttle, etc) are in ideal contact. In reality, the resistance is of the transitions (electrical and thermal) have finite values and this introduces a number of corrections to the distribution of the potentials. The dangerous areas can be simulated on the condition that the outer jacket has the zero potential.

Figure 6 shows the total distribution of the strength of the electrical field. The section of this field (the electrode with the adjacent region of the furnace) is shown in Fig. 7. The figures show the distribution of the vector of the electrical strength since the nature of this field is identical with the field of the vector of current density. The accompanying characteristics are linked by the dependence $E = \rho(T)j$, where E is the strength of the

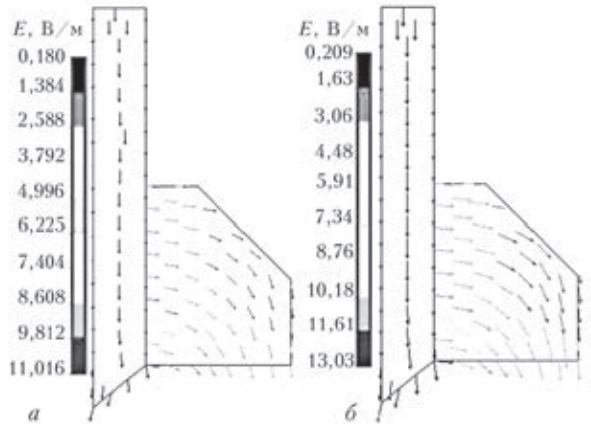

Fig. 7. Distribution of the vector of the strength of the electrical field in the region of the electrode and in the adjacent section in the regime II without the throttle (a) and with the throttle (b).

electrical field; $\rho(T)$ is the dependence of specific electrical resistance on temperature; j is current density.

The arrows in Fig. 7 show the direction of passage of current, and the length of the arrows corresponds to the level of the strength

of the electrical field (and, therefore, also current density). The highest values of the strength of the field are found at the ends of the electrodes, especially the upper electrode.

The maximum values of current density at the end of the upper electrodes in the regime I reached 16.7 [V/m]/0.008 [ohm·m] = 0.208 [A/cm^2]. In the model with the throttle the current density is 0.245 A/cm^2. It should be mentioned that the actual current density is approximately 6 times higher. This is associated with a special features of the proposed model (the actual voltage drop as shown previously is approximately 6 times lower). Thus, the actual maximum values of the current density should reach 1.25 without the throttle and 1.40 7A/cm^2 with it. These values may be made more accurate using areliable experimental data on the parameters of the conditions and electrical properties of the elements of the furnace and the processed thermal anthracite.

Conclusions

1. The experimental results show that the electric thermal models of the furnace of the electric calcinator, regardless of only the small amount of the experimental data, reflect the important features of the process confirmed by experiments. The model makes it possible to indicate the sections of the elements of the furnace most stressed in the thermal and electrical sense.

2. It has been shown that the stationary model can not be used to obtain the output values of the electrical resistance of thermal anthracite. This is associated with the hysteresis nature of the thermal properties of thermal anthracite which cannot be simulated in the stationary model. A non-stationary model is required for stricter formulation.

3. The temperature field of the model with the throttle explains the high homogeneity of the electrical properties of thermal anthracite. This is associated with the existence of a narrow temperature range in the continuous transverse (horizontal) cross-section of the furnace in the region of the throttle.

4. The process of sampling completed thermal anthracite in the lower part of the furnace shaft was investigated using the experimental data. The more accurate description is possible taking into account the phase transition in the region of exit of thermal anthracite or by investigating the real dynamics of its movement in the furnace shaft. The solution of the non-stationary problem is possible to investigate the process of the electric calcinator reaching the working regime (heating of the furnace) in order to minimise the general losses of electric energy.

5. It is interesting to investigate the problem optimisation of the geometrical parameters of the furnace (the dimensions and geometry of the upper and lower electrodes, and also of the throttle) and the electrical parameters of the conditions in order to minimise the specific consumption of energy. However, a large number of experimental data is required for efficient numerical modelling.

One of the advantages of the numerical modelling is the reduction of the number of expensive full-size experiments required for the determination of the optimum operating conditions of the system.

References

1. Pal'ti, A.M. and Yurchenko, D.D., Svar. Proiz., 2006, No. 2, 12-15.
2. Patent 89263, Ukraine, MPC B 21k., 31.03.2008, Byul. No. 3.
3. Chalykh, E.F., Technology and equipment for electrode electric carbon plants, Metallurgiya, Moscow, 1972.
4. Agroskin, A.A., Thermal and electrical properties of coal, Metallurgiya, Moscow, 1959.
5. Kutateladze, S.S., Heat transfer and hydrodynamic resistance, a handbook, Energoatomizdat, Moscow, 1990.
6. Lakomskii, V.I., Dop. NAN Ukraini, 2004, No. 9, 94–98.

Advances in Electrometallurgy 2011 ***9*** *(2) 109–114*
Translated from Sovremennaya Elektrometallurgiya 2011 ***9*** *(2) 50–55*

NEW MATERIALS

Titanium aluminide coatings on 12Cr18Ni10Ti steel with a barrier layer of titanium nitride

M.V. Arshuk, A.V. Mikitchuk, V.G. Zhizhnyak and M.V. Karpets

Kiev Polytechnical Institute, National State Technical University; International Centre for Electron Beam technologies; E.O. Paton Electric Welding Institute, Kiev

Abstract: Phase and chemical compositions, structures and microhardness of diffusion coatings, containing titanium and aluminium, were studied on samples of steel 12Kh18N10T. Depending on the type of treatment the multilayer coatings on titanium carbide and nitriDe base, intermetallics and oxides of titanium, aluminium, nickel, chromium, iron, as well as solid solutions of titanium and aluminium in austenite are formed on steel. It was found that during chemical-thermal treatment the titanium-nitride layer has a function of a barrier, delaying the aluminium and titanium diffusion into a base and the base components – into a coating.

The increase of the heat resistance and microhardness of the surface layers of 12Cr18Ni10Ti steel is an important task [1, 2]. Since the possibilities of volume alloying of the steel are limited, the solution of the problem using the methods of surface alloying is highly promising [3–5]. In this case, the metals and alloys are subjected to diffusion chemical-thermal treatment resulting in the formation on the surface of the substrate of a layer which differs from the initial material in its composition.

The solution of the task formulated above to obtain complex coatings on 12Cr18Ni10Ti steel, combining creep and corrosion resistance with high wear resistance, is of scientific and practical interest. It has been shown that complex saturation of the alloys with titanium and aluminium is highly promising [4, 6, 7]. The titanium-aluminide coatings, produced on commercial iron, carbon steels, and creep-resisting alloys, are characterised by satisfactory wear resistance and high creep resistance in the atmosphere of the products of combustion of organic fuel, containing sulphur and seawater vapours.

The reserve of creep resistance, the possibilities of using the coating in the conditions of friction and the effect of corrosive media are determined not only by the phase and chemical composition, the type of structure, but also by the nature of diffusion processes in the coating and at the coating-base material interface, and also the coating-environment interface.

The shielding properties of the creep-resisting coatings depend on the mass fraction of aluminium and, in most cases, decrease with the reduction of the fraction as a result of oxidation of aluminium in contact with the

atmospheric oxygen, and the diffusion of aluminium into the substrate and of the elements of the substrate into the coating [3]. Similar phenomena can also take place in the conditions of contact interaction of the coating with the process material, for example, in friction. This may be accompanied by diffusion transfer of the process material into the coating and vice cersa, which results in the rapid wear of the coating and its failure [8, 9].

The undesirable diffusion of chemical elements into the coating can be prevented or reduced by producing barrier layer is characterised by low or no permeability with respect to the atoms of the contacting substances. In addition, the barrier layer should retain the required properties in the given temperature-time range, should be characterised by efficient adhesion with both the substrate under coating [4]. The barrier coatings are represented by the coatings produced directly during saturation or in the course of service [3, 4, 6, 9].

Analysis of the experimental results [6, 10, 11] shows that titanium alitizing of nitrided commercial iron or carbon steels is accompanied by the formation of multilayer coatings in which the components, containing aluminium, are distributed on the outer side of the diffusion zone and are restricted by the internal layers of TiC carbide and TiN nitride. As indicated by the experimental results in [6, 10, 11], the main barrier function in the composition of the layers is played by the TiN layer, preventing the penetration of aluminium into the base material.

Further development of the creep resisting materials with a wide range of the functional properties should take place primarily in the direction of development of new multicomponent coatings ensuring high creep resistance of layers with the barrier properties of other layers.

In this study, titanium alitizing was carried out on specimens of nitrided 12Cr18Ni10Ti steel and the specimens of a steel with the layer of TiN, deposited on the surface by the method of reactive ion-plasma sputtering.

Nitriding of the 12Cr18Ni10Ti steel was carried out in dissociated ammonia at a temperature of 540°C over 20 h. The titanium nitride was deposited by the method of reactive ion-plasma sputtering in equipment VU-1B for 0.33 h at the preheat temperature of the specimens prior to spraying of 560-600°C, the pressure of the the reaction gas of $2.5 \cdot 10^{-2}$ Pa, arc current 100 A, the applied bias potential was +150 V. Preliminary cathode sputtering was carried out for 1 min at a current of 3 A.

Titanium alitizing was conducted with the powder method in containers with a fusible gate at reduced pressure. The specimens with the coatings were investigated by x-ray diffraction, x-ray spectrum microanalysis, metallographic analysis, and hardness methods.

The phase composition and some properties of the alitized layer and of the layer of titanium nitride TiN on the 12Cr18Ni10Ti steel, produced in the treatment conditions, used in the investigations, are presented in Table 1.

The presence of Fe_3O4, Fe_4N, Fe_2N and CrN was confirmed on the outer side of the nitrided layer. They analysis of the internal side of the nitrided layer shoulder presence of CrN and Feγ (N). The thickness of the nitrided layers in different zones of the specimen was varied from 100 to 140 μm. The difference in the values of the thickness of the diffusion layer in individual zones of the specimens was determined primarily by the effect on the process of saturation of the oxide films of chromium at the given saturation temperatures, differing in high density and stability.

The titanium nitride, deposited on the specimens of 12Cr18Ni10Ti steel, on the surface and in the cross-section is characterised by the typical yellow-gold colour, which corresponds to the composition close to the stoichiometric [3,12]. The latter is confirmed by the results of x-ray diffraction analysis of the coating according to which the period of the crystal lattice of TiN is close to stoichiometric and equals 0.4249 nm.

The phase composition of the coating on the specimens of titanium-alitized 12Cr18Ni10Ti steel is characterised by the

Table 1. Phase composition and properties of the coatings on 12Cr18NiTi steel

Type of treatment, t, °C; time, h	Phase composition	Crystal lattice parameters, nm		Coating thickness,mm	Microhardness, MPa
		a	c		
Alitizing, 540, 20	Fe_3O_4	0.8385	—	45.0. 60.0	10.0... 15.5 1
	Fe4N	0.3700	—		
	Fe2N	0.4798	0.4419		
	CrN	0.4152	—		
	CrN	0. 4149	—	60.0. 80.0	16.0. 18.5
	Fey(N)	0.3618	—		
TiN (reactive ion-plasma sputtering); 560...600; 10.33	TiN	0.4249	—	5.5. 6.0	21.0
	Fe_2Ti	0.4825	0.7840	39.0. 42.0	5.5... 6.0 1
	Ti_4Fe_2O	1.1267	—		
	TiC	0.4180	—	0.5... 1.0	–
	Feγ(Ti, Al)	0.3560	—	70.0. 80.0	3.5. 2.0
Titanium-alitizing after nitridingm 1050; 3	Fe_2Ti	0.4987	0.8163	7.0. 9.5	9.5. 12.5
	Ti_4Fe_2O	1.1441	—		
	TiN	0.4261	—	5.0. 7.0	20.5
	Fey	0.3584	—	50.0. 70.0	4.5. 2.5
	CrN	0.4150	—		
Titanium-alitizing after deposition of TiN (reacrive ion-plasma sputtering, 1050, 3	Fe_2Ti	0.4825	0.7840	5.0. 7.0	6.0. 6.5
	Ti_4Fe_2O	1.1267	—		
	TiN	0.4267	—	5.0	23.0

zone of compounds Ti_4Fe_2O, Fe_2Ti, TiC, and by the zone of the solid solution of titanium and aluminium in austenite. The results of x-ray spectrum microanalysis and layer x-ray diffraction analysis show that the layer of the titanium carbide 0.5-1.0 μm thick separates the zone of the compounds from the solid solution. The concentration of titanium and aluminium at a distance of 60 μm from the surface in the solid solution equals 2.5 and 2.0 wt.%, respectively. The elements of the substrate (iron, nickel, chromium) are found in the zone of these compounds (Fig. 1).

Thus, it may be concluded that the TiC layer does not fulfil efficiently the barrier functions to reduce the extent of diffusion penetration of titanium and aluminium into the base material.

Layer x-ray diffraction analysis of the coatings after combine treatment (alitizing with subsequent titanium alitizing, and also the deposition of the TiN layer followed by titanium alitizing) shows that in both cases, the binding zone has the same phase composition. It is the titanium nitride, situated at the interface with the brazed material and on the outer side of the diffusion zone (Fe_2Ti and Ti_4Fe_2O).

The period of the crystal lattice of the TiN layer after titanium alitizing greatly increases as a result of additional alloying, primarily with aluminium. The periods of the lattices

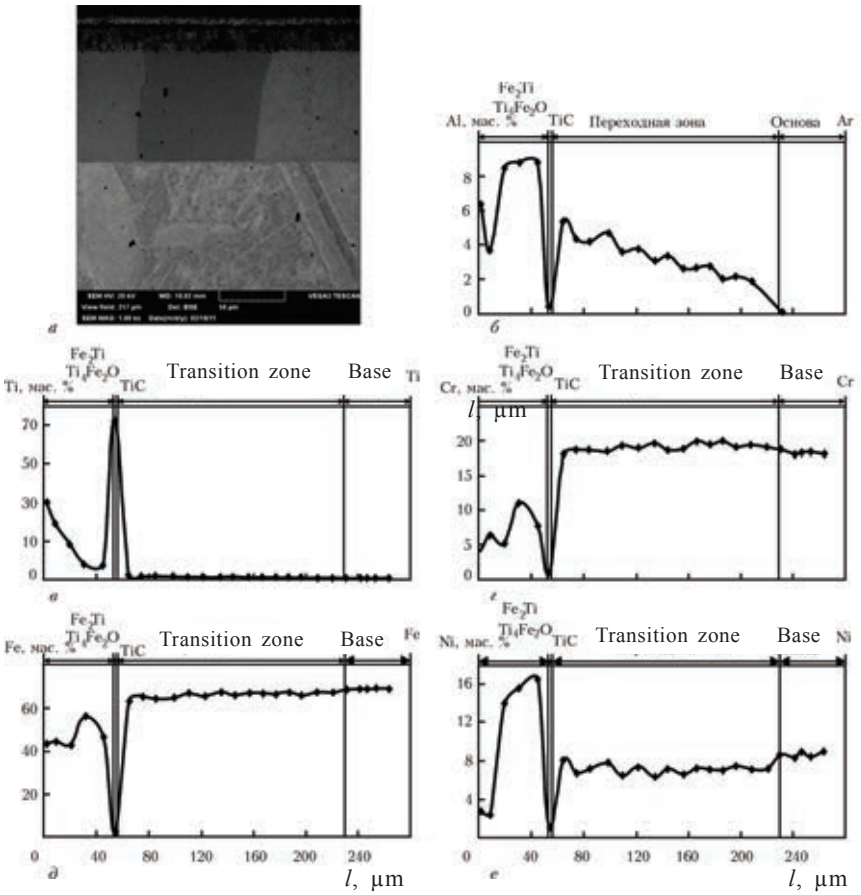

Fig. 1. Microstructure (a) and the distribution of elements in the thickness of the coatings on 12Cr18Ni10Ti steel (b-c) after titanium-alitizing: l is the distance from the surface.

of the nitride phases, produced by different methods, are almost identical.

The experimental results in the investigations of the kinetics of growth of the TiN layer in nitriding-titanium alitizing show the parabolic dependence of the thickness of the layer on the saturation time. The thickness of the TiN layer, formed in titanium-alitizing, does not change in subsequent saturation. It may be assumed that the barrier properties of the TiN layer in titanium-alitizing of the nitrided steel increase with increase of the thickness of the layer of TiN. In particular, this circumstance also was the reason for the difference in the chemical composition of the complex coatings, produced by different methods.

The results of x-ray spectrum microanalysis of the specimens show that the distribution in the layer of the saturating elements and the substrate elements for the three types of coatings has a number of common features (Fig. 1-3).

The maximum concentration of titanium in the coating was recorded at a certain distance from the surface in the layers of titanium carbide or titanium nitride.

A large difference of the titanium-aluminide coating in comparison with the coatings containing TiN is the almost complete absence in the structure of the TiN coatings of the solid solution of titanium and aluminium in austenite. In addition, the TiN barrier layer reduces the extent of penetration of the components of the base material into the coating. The most efficient barrier was the TiN layer produced by the method of reactive ion-plasma sputtering. The diffusion layer of TiN in the nitrided-titanium-aluminide coating reduces the rate of penetration of iron, nickel, chromium into the layer of the compounds to a lesser extent than the deposited TiN layer

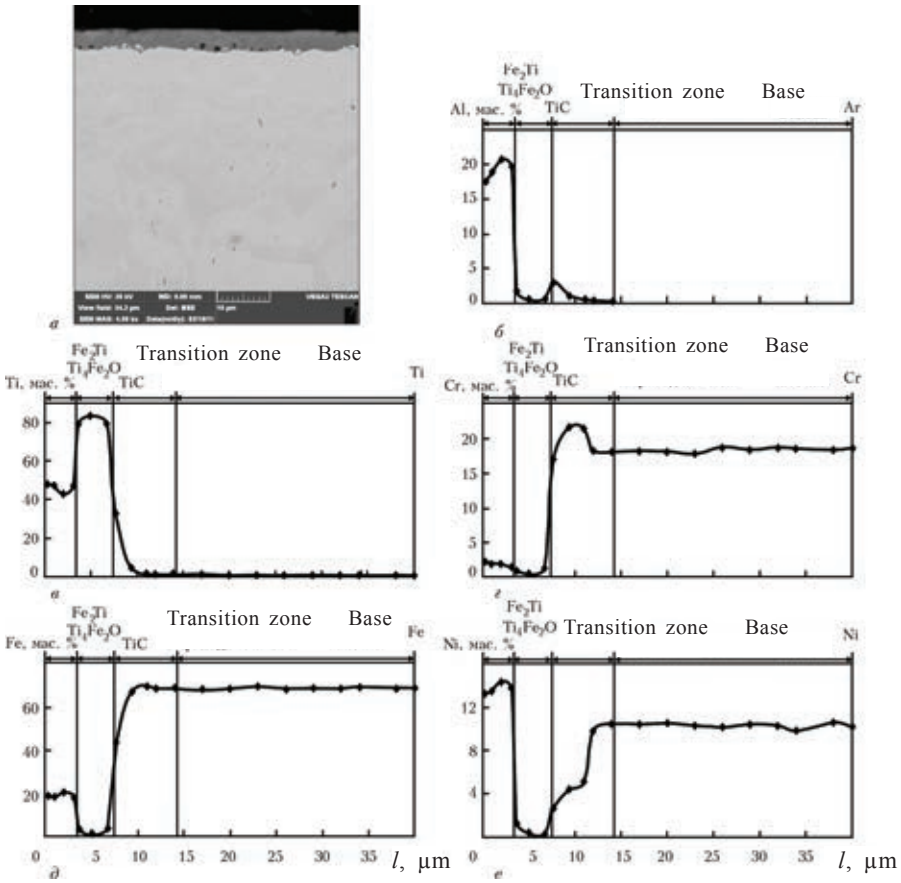

Fig. 2. Microstructure (a) and the distribution of the elements in the thickness of the coatings of 12Cr18Ni10Ti steel (b-c) after nitriding-titanium alitizing.

because this layer formed and increased its thickness during titanium-alitizing. For example, the chromium concentration of the titanium-alitizing layer was 4.5-12.5, in the nitrided-titanium alitizing layer it was 2.5-4.0, and in the coating with the deposited titanium nitride 0.5 wt.%.

The experimental results show that the microhardness of the metal of the zone of the compounds Fe_2Ti, Ti_4Fe_2O in the nitrided-titanium alitizing layer on 12Cr18Ni10Ti steel is 9.5-12.5 GPa which is higher than in the metal of similar zones after titanium-alitizing or titanium-alitizing of the titanium nitride deposited in advance in the substrate. It may therefore be assumed that the increase of the microhardness of this coating is determined by nitrogen which in nitriding-titanium alitizing not only forms the layer of the TiN nitride but also forms the Ti_4Fe_2O compound and, replacing part of the oxygen atoms, supports the formation of $Ti_4Fe_2OxN1 - x$ compound.

Conclusions

1. The experimental results show that in titanium-alitizing of the specimens of the 12Cr18Ni10Ti annealed steel (in the initial condition, after preliminary nitriding and on the deposited TiN layer) multicomponent coatings Fe_2Ti, Ti_4Fe_2O, TiN, TiC form.

2. It was also shown that the layer of the TiN compound plays the role of a barrier which greatly reduces the content of iron, nickel and chromium in the coating, and also greatly reduce is the rate of diffusion of titanium and aluminium into the base. The microhardness of the TiN layer in the complex compounds is 20.5-23.0 GPa, and that of the diffusion zone of the compounds 5.5-12.5 GPa.

3. The variants of the multilayer coatings,

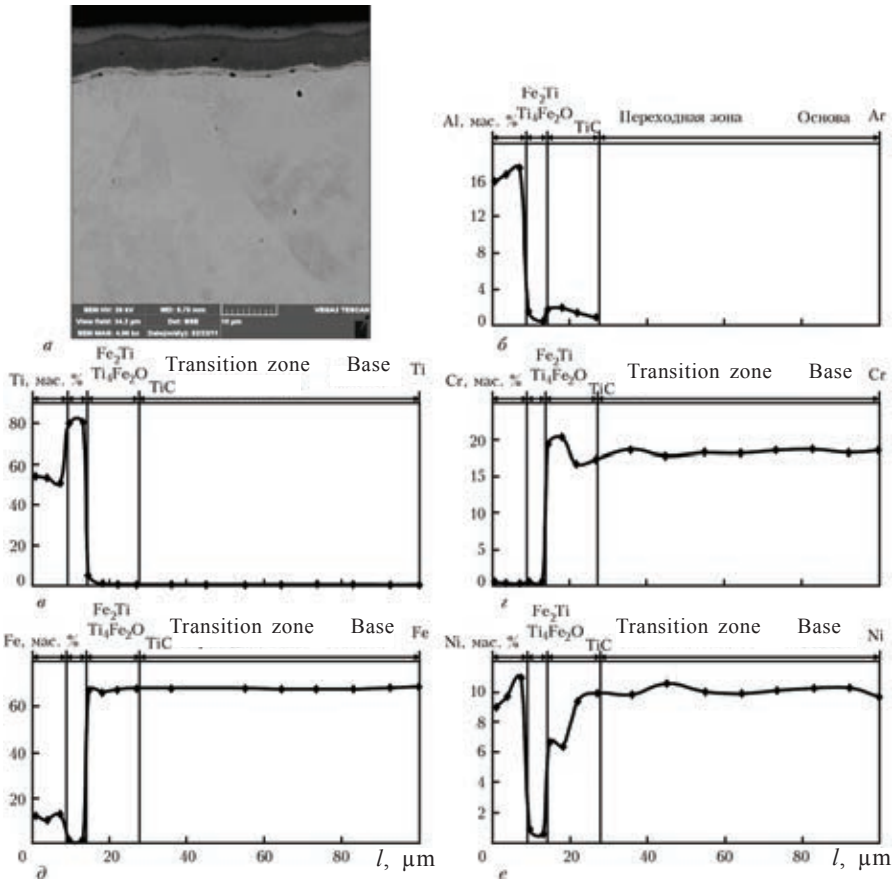

Fig. 3. Microstructure (a) and the distribution of elements in the thickness of coatings on 12Cr18Ni10Ti steel (b-f) after titanium-alitizing with the deposited layer of Ti N by the method of reactive ion-plasma sputtering.

produced as a result of titanium-alitizing of the 12Cr18Ni10Ti nitrided steel, and also the steel on which the TiN layer was previously deposited, are promising as regards the composition, structure, properties and presence of the barrier layer of titanium nitride in the coating, and can be used for application as creep- and corrosion resisting antifriction materials.

References

1. Khimushin, F.F., Creep resisting steels and alloys, Metallurgiya, Moscow, 1969.
2. Priimak, E.Yu., et al., Metalloved. Termich. Obrab. Met., 2009, No. 9, 21–24.
3. Kolomytsev, P.T., Creep-resisting diffusion coatings, Metallurgiya, Moscow, 1979.
4. Borisenko, G.V., et al., Chemical-thermal treatment of metals and alloys, a handbook, Metallurgiya, Moscow, 1981.
5. Golovanov, A.V., et al., Metalloved. Termich. Obrab. Met., 2008, No. 6, 42–45.
6. Khizhnyak, V.G., et al., Naukovi visti NTUU KPI, 2009, No. 9, 92–96.
7. Kaidash, H.G., et I., In: Creep-resisting coatings for structural materials, Nauka, Leningrad, 1977, 195-199.
8. Loskutov, V.F., et al., Diffusion carbide coatings, Tekhnika, Kiev, 1999.
9. Vereshchaka, A.S. and Tret'yakov, I.P., Cutting tools with wear-resisting coatings, Mashinostroenie, Moscow, 1986.
10. Khizhnyak, V.G., et al., Naukovi visti NTUU KPI, 2008, No. 6, 83–88.
11. Arshuk, M.V., et al., Problemi tertya ta znoshuvaniya, 2009, No. 51, 123–131
12. Tom, L., Carbides and nitrides of transition metals, Mir, Moscow, 1974.

Advances in Electrometallurgy 2011 ***9*** *(2) 115–121*
Translated from Sovremennaya Elektrometallurgiya 2011 ***9*** *(2) 56–60*

Special features of ion-plasma metallising of ceramic powders

I.V. Smirnov

Kiev Polytechnical Institute, Kiev

Abstract Effect of conditions of ion-plasma metallization on the concentration of ions of titanium, aluminium and copper in the metallic plasma flow was studied. Suggested are the relationships allowing determination of time, required to attain the preset temperature on the powder particle surface and to produce a metallic film of the required thickness.

The production of advanced composite materials requires the development of a wide range of initial powders, often in small batches. It is therefore necessary to develop flexible and universal processes, which result in the required properties of the powder materials.

One of the directions of solving this problem is the application of the technologies of metallising of powders by vacuum condensation which can be used to metallise almost any metals and alloys, to change easily the thickness of the coating, and also the temperature in the contact zone from 297 to 1000 K or even higher.

As a result of the application of cathodes produced from different materials and changes of the composition of the medium in the working space of vacuum equipment, it is possible to produce from simple components multilayer, discrete, gradient and nanocrystalline coatings [1].

At the present time, vacuum metallising of the powders is carried out by electron beam, resistance, magnetron and ion-plasma deposition of coatings [2–5]. Electron beam deposition in a vacuum of $2 \cdot 10^{-3}$ Pa has been used to produce films of metals (molybdenum, titanium, vanadium, etc) on the powder of synthetic diamond and the cubic borron nitride to increase the durability of diamond tools [2]. The method of resistive evaporation was used in [3] for the metallising of graphite powder with copper.

Metallising of the powder by these methods is complicated by the typical direction of the flow of vapours from top to bottom from the evaporator and the powder particles during metallising are in the free falling state.

A more rational method of distribution of the evaporator (targets) and the surface to be treated as can be realised using the magnetron sputtering system.

The method of magnetron sputtering has been used to produce films of nickel and tin with a thickness of 5–10 μm on the particles of quasi-crystalline powders in the production of thick composite materials with higher physical-mechanical properties [5].

From the viewpoint of the technological and design possibilities, the most efficient method for the deposition of coatings on powders is the method of ion-plasma spraying which makes it possible to control in a wide range the parameters of the process and the condensate properties at a result of the presence of the highly ionised component in the products of cathode erosion and can be used to produce high-quality coatings from different materials with the high adhesion of the coating with the processed surface [6, 7].

The efficiency of the ion-plasma method of deposition is showed in deposition of metallic films of aluminium and nickel on the ceramic powders of the oxides of aluminium and zirconium for thermal spraying of the protective coatings [8]. The plasma coatings, produced using these powders, are characterised by high wear resistance and bonding strengths with the substrate.

The powders as objects for metallising, in contrast to the thick materials, have a number of the following technological special features in deposition of the coatings:

firstly, since the process of heat transfer in vacuum is complicated, the powder particles may be overheated as a result of the generation of condensation heat of the metal;

secondly, the powders, especially the fine fraction powders, are susceptible to 'sticking' which becomes more intensive in the process of the position of the vapour flow so that it is necessary to take special measures to prevent aggregation of the particle;

thirdly, the developed surface of the powders is a source of generation of the adsorbed moisture and gases. This influences the pumping process and formation of deep vacuum.

Therefore, in metallising of the powders it is especially important to determine correctly the technological conditions because the quality of the produce films on the powder particles depends primarily on the parameters of the metallic plasma flow, temperature in the contact zone and metallising time.

The aim of the present study was to determine the optimum conditions and the conditions of ion-plasma deposition of functional films on the ceramic powders by determination of the parameters of the metallic plasma flow and the time dependence of the metallising process.

The investigations of the plasma parameters and the determination of the relationship of the parameters with the properties of the coatings have been carried out in a large number of studies, which are analysed in [9].

The selection of the conditions of the position of iron-plasma coatings (arcing current, bias potential, the distance from the cathode of the surface of the substrate, pressure in the vacuum chamber) depends on the nature of the deposited material. Each material has its own limiting current. The lower boundary characterises the minimum value of arc current at which the arc discharge is self-sustaining (threshold current). The increase of the current above the maximum value results in the increase of the amount of the vapour and droplet phase in the products of erosion of the cathode material and this has a detrimental effect on the quality and composition of the coating.

The evaporated materials include titanium, aluminium, copper, which have different values of threshold current and evaporation mechanism. The coatings produced from these materials were deposited on the particles of powders Al_2O_3, ZrO_2, WC, used in the production of creep- and wear-resisting coatings by thermal spraying, surfacing, sintering, etc.

The metallising of the powders was carried out in ANGA-1 ion plasma spraying equipment fitted with a special drum-type device for mixing the powder [10]. The technology, equipment and the processes, taking place during cladding of the powder by this method, have been studied in [11].

To determine parameters such as electron temperature, the concentration and temperature of the ions of the evaporated metals, investigations were carried out using the approaches based on the determination of the volt-ampere characteristic of a single probe [12].

The conditions of ion-plasma metallising were determined on the basis of the maximum concentration of the ions in the flow of metallic plasma. The concentration of the ions of the evaporated metals was calculated on the basis of the volt-ampere probe characteristics using the Bohm equation:

$$N_i = \frac{2.5 J_{in}}{qS\sqrt{2kT_i / M_i}}, \quad (1)$$

where J_{in} is the ion current on the probe at the floating potential of the plasma; q is the particle charge; S is the surface area of the

probe; k is the Boltzmann constant; T_i is the particle temperature; M_i is the mass of the ion.

The graphical dependences of the concentration of the ions of titanium, copper and aluminium on the axis of the plasma flow in relation to the spraying distance and the vacuum arc current, calculated using equation (1), are presented in Fig. 1 and 2.

The graphs, shown in Fig. 1, indicate that the concentration of the titanium ions is in the range $8\cdot10^{16}\ldots7\cdot10^{15}$ cm^{-3}, the aluminium ions $7\cdot10^{16}\ldots5\cdot10^{14}$ cm^{-3} in relation to spraying distance. According to Fig. 2, the concentration of the titanium ions reaches the maximum value at an arc current of 120-140 A, and that of copper starts to decrease with increase of the arc current above 100…110 A. For aluminium, this tendency was already recorded at 80–90 A, and there was also a large decrease of the content of the ions when the current was increased above 120 A.

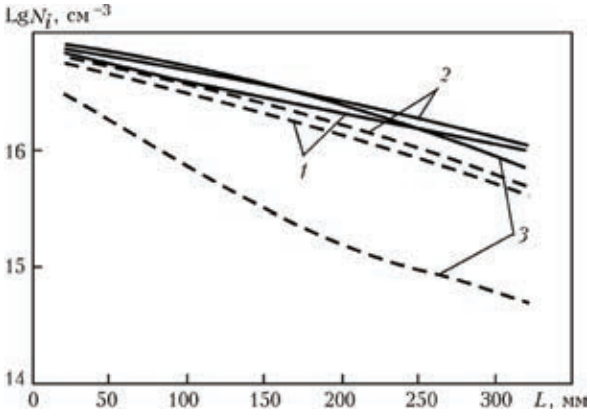

Fig. 1. Dependence of the concentration of the islands of titanium (broken line) and aluminium (solid line) and spraying distance for different arc current, A: 1) 60; 2) 100; Si) 140; L is the distance from the cathode to the substrate.

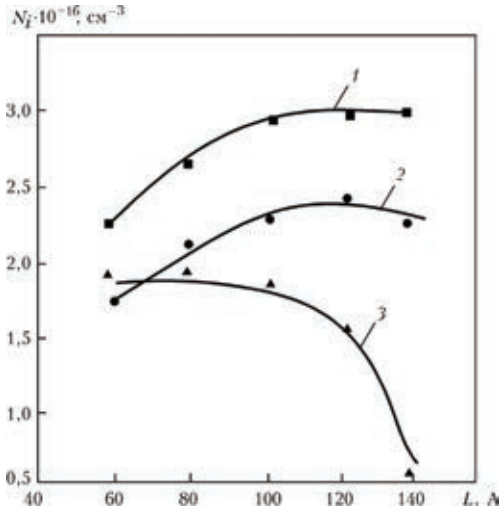

Fig. 2. Dependence of the concentration of the ions of titanium (1), copper (2) and aluminium (3) in the metallic plasma of the appropriate metals in vacuum arc current.

The evaluation of the temperature of the powder particles during metallising is a complicated and very important procedure. The deposition of the coatings in vacuum by the ion-plasma method is accompanied by heating of the substrate surface with increasing intensity and this may cause undesirable changes in the structure and composition of the material. This is accompanied by changes of temperature in a wide range. This depends on the design elements and the working conditions of vacuum equipment.

In the stationary evacuated mass of the powders, heat transfer is carried out only by means of contact heat conductivity of the particles and radiation. In transfer of heat by contact heat conductivity, the entire thermal resistance is concentrated in the contact area of the particles. Heat conductivity is determined by the physical characteristics of the powder material, density, the geometry of the charge, and is independent of the particle size.

In heat exchange by radiation, the layer of the powder is a system of thermal screens whose number depends on the radius and geometry of the charge. Thus, as a result of the low contact heat conductivity in the screening effect in radiant heat transfer, the effective heat conductivity of the layer is approximately $1\cdot10^{-2}\ldots1\cdot10^{-3}$ W/(m·K).

The temperature of the powder particle surface can be evaluated to the first approximation on the basis of the thermal balance equation which has the following form for a spherical powder particle:

$$\frac{\pi d^2}{4}P_{sp} = cm\frac{dT_s}{dT} + \left(T_s - T_0\right)I\left(d\right), \qquad (2)$$

where d, c, m are respectively the diameter, heat capacity and mass of the powder particle; P_{sp} is the specific absorptivity; T_s is the temperature on the surface of the powder

particle.

$$I(d)=\int_0^2 \frac{2\pi x dx}{\frac{2}{\lambda_1}\sqrt{\left(\frac{d}{2}\right)^2-x^2}-\frac{1}{\lambda_2}\left(\frac{d}{2}-\sqrt{\left(\frac{d}{2}\right)^2-x^2}\right)}=$$
$$=\frac{\pi\lambda_1\lambda_2 d}{2\lambda_1+\lambda_2}+\frac{\pi d\lambda_1^2\lambda_2}{(2\lambda_1+\lambda_2)^2}In\left(\frac{2\lambda_2}{\lambda 1}\right),$$

Here λ_1, λ_2 is the heat conductivity of respectively the powder particle and the environment; x is the integration variable.

After appropriate substitutions and transformation of equation (2), we obtain

$$\frac{dT_s}{dt}=-\frac{6}{c\rho\pi d^3}T_s I(d)+\frac{6}{c\rho\pi d^3}T_0 I(d)+\frac{3}{2c\rho d}P_{sp}. \quad (3)$$

The solution of equation (3) with the initial condition $T(0) = T_0$ taken into account, has the form

$$T(t)=\left(T_0+\frac{b}{a}\right)e^{at}-\frac{b}{a}, \quad (4)$$

where

$$a=-\frac{6\lambda_1\lambda_2}{c\rho h^2(2\lambda_1+\lambda_2)}\left(1+\frac{\lambda_1}{2\lambda_2+\lambda_1}\ln\frac{2\lambda_2}{\lambda_1}\right);$$
$$b=-aT_0+\frac{3}{2c\rho d}P.$$

Thus, from equation (4) we determine the time to reach the given (permissible) temperature of the powder particles of the given fraction

$$t=\frac{1}{a}\ln\left(\frac{aT_s+b}{aT_0+b}\right). \quad (5)$$

The graphical dependences of the metallising time on the diameter of the powder particles of aluminium oxide for the given temperatures is shown in Fig. 3.

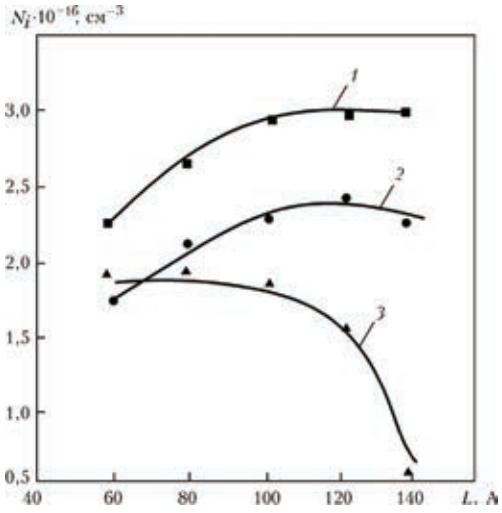

Fig. 3. Theoretical dependences of metallising time on the diameter of the particles of the aluminium oxide powder at the following temperatures on the surface of the particles, °C: 1) 300; 2) 250; 3) 200.

On the basis of Fig. 3 be concluded that the temperature of, for example, 300°C, on the surface of the powder particle with a diameter of 16 μm can be reached within approximately 20 s. In this case, it is necessary to take appropriate measures to stabilise the temperature of the powders based on intensive mixing of the powder, periodic removed from the zone of effect of the metallic plasma flow or in cyclic metallising.

A special feature of metallising of the powders is the deposition of a coating on a large surface (10–100 m^2 or greater, depending on the amount of the powder and its specific surface). For this purpose, it is necessary to increase the duration of the metallising process as a result of evaporation of a large amount of metal. Therefore, the process of metallising of the powder is characterised by the effective rate ve of the growth of the thickness of the shell on the particles. Using this rate, determined experimentally by means of the condensation rate on flat reference specimens, it is possible to determine the time required for depositing a film of the given thickness of the particles of a specific powder fraction:

$$\tau = \int_0^h \frac{dh}{v_{ef}} = \int_0^h \frac{M_p S_{part}}{M_{part} S_p v_c} dh, \quad (6)$$

where h is the thickness of the film deposited on the powder particles, μm, v_c is the rate of condensation of the metal of the film on the flat surface, μm/min; S_p, S_{part} is the area of respectively the layer of the powder and the surface of an individual particle, mm^2; M_p, M_{part} is the mass of respectively the loaded powder and the individual particle, g.

Assuming that the powder particles are spherical, after appropriate substitution and integration of equation (2) we obtain

$$\tau = \frac{M_p}{\rho S_p v_c} \left(\frac{R+h}{R} \right)^3, \quad (7)$$

where r, R is respectively the density and radius of the powder particles.

As indicated by equation (7), the metallising time for obtaining the required thickness of the film depends both on the mass of the loaded powder and this faction, and also on the productivity of the evaporator in the area of the loading (mixing) equipment.

The graphical dependences of the metallising time on the diameter of the powder particles for different materials are shown in Fig. 4.

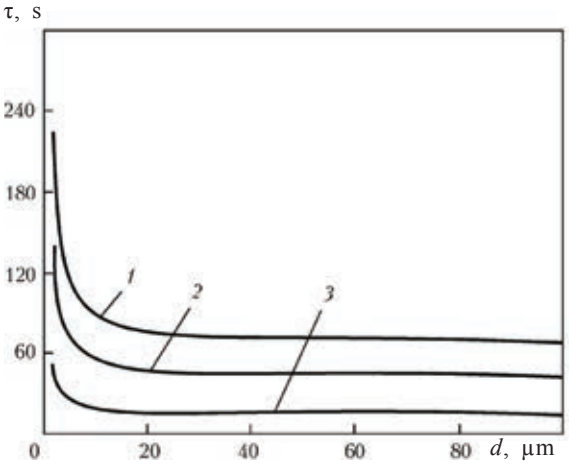

Fig. 4. Theoretical dependences of metallising time on the diameter of the particles of the powders of aluminium oxide (1) and zirconium oxide (2) and also tungsten carbide (3).

Analysis of Fig. 4 shows that the diameter of the powder particles has a strong effect on the metallising time. When the diameter is smaller than 10 μm, the metallising time rapidly increases and the condensation rate decreases, and when the radius is reduced below 1 μm the metallising time increases to the technologically unacceptable level. Therefore, when calculating the metallising time, it is important to take into account both the mass and the particle size of the powder. For example, the metallising time of particles with a diameter of 20–100 μm to produce films with a thickness of 1 μm should not exceed 60–80 min at a mass of 300 g. The resultant dependences of the metallising time on the film thickness H are in good agreement with experimental data, presented in Table 1.

Thus, the maximum amount of the powder of the given grain size, loaded into the equipment, is linked with the dimensions of the mixing equipment and the power of the evaporator. To increase the proactivity of equipment, it is necessary to increase rationally the amount of metal, evaporated in unit time. However, even this method has limitations because of the formation of the droplet phase in the products of cathode erosion and increase of the temperature of the powder particles.

To evaluate the effect of the technologi-

Table 1. The chemical composition and thickness of metallic films H

Spectrum No.	O	Al	Ti	Zr	H, nm	
					Ti	Al
Aluminium oxide powder						
1	41.72	47.04	11.23	—	162	177
	37.52	48.31	14.17	—	197	165
3	23.85	55.61	20.54	—	266	577
	22.23	58.54	19.23	—	251	633
Zirconium oxide powder						
1	37.12	16.77	3.25	42.86	41	289
	44.10	0.14	4.86	50.90	70	30
3	29.95	2.33	5.99	61.74	72	51
4	34.82	3.21	2.20	59.76	29	69

Comment. in all spectra, the total number of elements is 100%

cal conditions of ion-plasma metallising on the composition, uniformity and thickness of the deposited metallic films on the ceramic powders, investigations were carried out using metallographic and electron scanning microscope analysis of the morphology of the surface and structure of the films, with the results presented in Figs. 5, 6.

Metallographic analysis of the metallised powders shows that the deposited films are uniform, have a stepped relief and are distributed uniformly on the surface of the powder particles. The spectroscopy data, presented in Table 1, indicate the high purity of the metallic condensates.

Figure 6 shows that this method is characterised by the sufficiently uniform deposition of the copper film on the surface of tungsten carbide particles with a diameter of 150–200 μm. The thickness of the film in this case was 4–6 μm at a metallising time of 20 min, which is in good agreement with the experimental data.

Analysis of the external appearance of the metallised particles and of the microstructure of the produced films shows the formation mechanism. The initial stage is characterised by the formation of spot-like areas in the form of islands on the nucleation centres represented by subsurface defects of the particles. Subsequently, increasing in diameter, the spot like formations merge together and form in the final analysis a continuous shell on the particle surface at a total content of the metal in the powder mass of 3–5 wt.%. The quality of the shell is determined by the regime parameters of metallising, the degree of dispersion, mass of the powder and the physical-chemical properties of the individual particles.

Conclusions

1. Experiments were carried out to determine the concentration of the islands of titanium, aluminium and copper in the metallic plasma flow. The variation of these parameters can be used to control the process of condensation of the metallic films on the ceramic powders. The limiting values of the discharge current resulting in the maximum concentration of the ions and in the formation of a uniform shell on the powder particles.

2. Mathematical models have been proposed for determining the time of establishment of the required temperature on the surface of the powder particles, and also the metallising time to produce the film of the required thickness. Consequently, it is possible to correct the technological conditions of ion-plasma metallising in relation to the mass of the loaded powder, it's fraction and productivity of the evaporator.

References

1. Kuchenko, Yu.V., et al., Fizicheskaya Inzh. Poverhnosti, 2004, No. 1, 102–108.
2. Naidich, Yu.V., et al., Poroshk. Metall., 1973, No. 9, 91–94.
3. Frishberg, I.V., ibid, 1981, No. 6, 1–5.

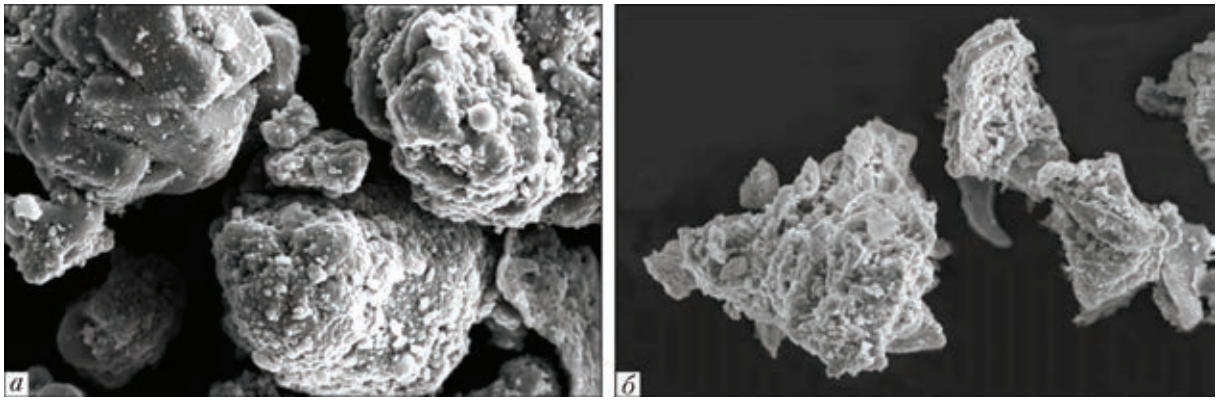

Fig. 5. Morphology of the particles of Al2O3 (a) and ZrO2 (b) powders, metallised with titanium and aluminium, × 2500.

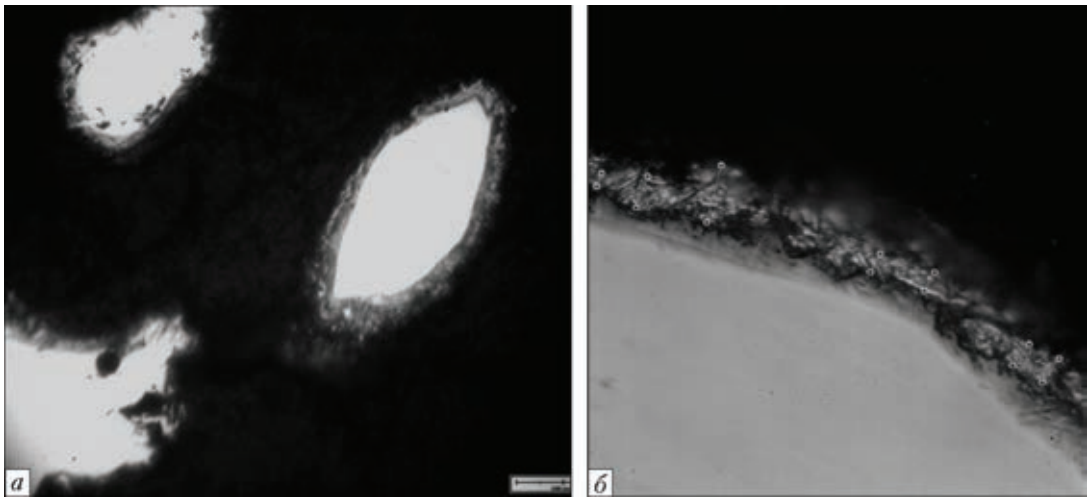

Fig. 6. Metallographic images of metallised particles of tungsten carbide (a) and the copper shell on their surface (b): a) × 500; b) × 1000.

4. Alimov, S.S., et al., In: Proceedings of the international conference Physics of plasma and plasma technologies, Minsk, 1997, vol. 4, 724–727.
5. Bezverkhii, E.D., et al., Nauchn. Sessiya MIFI-2010, vol. 4, MIFI, Moscow, 2010, 36–38.
6. Mrochek, Zh.A., et al., Fundamentals of the technology of formation of multicomponent vacuum electric arc coatings, Navuka i tekhnika, Minsk, 1991.
7. Sharonov, E.A., et al., Proceedings of the sixth International conference: Films and coatings, Proc. Int. Conf., St Peterburg, 2001, 146–149.
8. Novikov, N.N., et al., Poroshk. Metall., 1979, No. 11, 24–28.
9. Khoroshikh, V.M., Fiz. Inzh. Poverkh., 2003, No. 1, 19-26.
10. Patent 41184m Ukraine MPK B22 F1/00, 12.5.2009, Byull. No. 9.
11. Kopilov, V.I., et al., Naukovi visti NTUU KPI, 2009, no. 3, 11–20.
12. Chernyak, V.Ya., et al., Measurement of the temperature of the plasma ions by the probe method, Kiev, 1989.

Advances in Electrometallurgy 2011 ***9*** *(2) 122–124*
Translated from Sovremennaya Elektrometallurgiya 2011 ***9*** *(2) 65–66*

Comparative evaluation of the accuracy of the methods of X-ray fluorescence anaysis and emission spectroscopy with inductively-coupled plasma in analysis of the composition of fluxes

L.N. Chubov, G.M. Grigorenko and V.V. Lakomskii

E.O. Paton Electric Welding Institute, Kiev

Abstract It was found that the emission spectral analysis with inductively-bound plasma provides the better accuracy in determination of flux composition as compared with X-ray fluorescent method.

In analyzing the content of elements in the metal and slag are interested not only researchers but also producers and consumers of these materials. If the metal is sufficient to define the elements of base and alloying, in the case of slag must have information not only on the elemental composition as the phase, i.e., compounds of elements with oxygen and halides. In the middle of last century, the elemental composition measured using methods of the so-called "wet" chemistry. With the development of instrumentation there were other methods of analysis.

The phase composition is established by means of X-ray analysis techniques, elemental – a set of methods, such as X-ray and emission – spectral. Each has its advantages and disadvantages. The choice of method of analysis is not only accurate but also the rapidity (for manufacturers in the first place, the speed of analysis for researchers – accuracy). Therefore, each method of analysis should be evaluated in terms of applicability to the specific situation in the study of the elemental composition of materials, primarily of flux and slag.

X-ray fluorescence analysis (XRF) has long been used in plant laboratories as a reliable method of nondestructive testing of metal products. Its distinguishing feature is the ease of sample preparation of monolithic samples and a short measurement time.

In parallel with this, the chemical composition of metals and alloys was analyzed using the method of atomic-emission spark or arc discharge.

Both methods together with significant production advantage of the short duration of the analysis have inherent drawbacks: first – poor reproducibility of measurements of powder samples, the second – a real lack of their quantitative analysis.

If in the same type of production methods influence the weaknesses are minimized, the scientific and applied studies of materials which tend to differ substantially in chemical composition and physical condition, these features become sharply negative value.

XRF is a relative method, relying on standard samples. For the past used mainly samples from the same manufacturing process, previously analyzed by chemical measure-

ments. In this regard, the method is inferior emission analysis ES-ICP, which produce multi-element standard solutions to a wide range of applications.

Using XPA, it is usually impossible to quantify the content of the elements below $1 \cdot 10^{-4}$%. In terms of the sensitivity the method does not compete with emission and absorption spectral analysis of liquid samples [1]. The accuracy of these methods is determined by the fluorescence intensity of the element in the sample and depends not only on its concentration, radiation and physical properties used to excite fluorescence emission, but also on the content and properties of other elements present. This mutual influence of elements present in the nature of the radiation gives rise to the so-called "matrix effect".

The latter, though manifested in the ES-ICP, but here it is a negative impact on the analysis of impacts at a much greater proportion of elements.

A weakness of XFA [2] are the difficulties in the manufacture of the samples of powdered materials for quantitative analysis. Varying over a wide range size distribution of raw materials, and are not always sufficient to meet the homogeneity of the XFA controlled batches have a negative impact on the reproducibility of the determination of elemental composition pressed into tablet samples. Obviously, in this case, the mineralogical composition and grain size of the sample and calibration samples should be identical as possible. It is not possible to comply with this condition outside the mass analysis

At the same time it should be emphasized that the XFA required different sensitivity, provides a cost-effective production cycle, and (most importantly) an operational non-destructive testing of steel products.The advantage of the analysis is able to selectively determine the composition of a thin surface layer of the alloy subjected to a hardening of physical and chemical treatment. In this respect, ES-ICP will not be able to compete with the short term even if the method of XFA instrumentation block laser sublimation material sample.

In [3] suggest the accuracy of XFA analysis of powdered materials closer to the level of measurements of solid samples by avoiding the operation of melting the crushed sample in a boron-containing smoothly followed by grinding and pressing, amorphous mass. Instead, increase the number of initial samples, previously subjected to the necessary degree of dispersion. As a consequence of the publication [3], optimal results are achieved in the case of approximately10 parallel measurements. At the same time it is pointed out that the analysis of related materials used use of ES-ICP in the two samples, and double the frequency of each provides at least two times better accuracy of results:

Analysis of FeMn samples gave ± 0.5% by ES-ICP versus ±(1...2)% in XFA.

The total advantage of ES-ICP in comparison with XFA in assessing the composition of the oxide and similar systems is confirmed by the results of the quantitative determination of elements in standard welding fluxes, produced in the milled state. From these data (Table 1) it follows that the the XFA results significantly different from both the regulatory indicators, as well as from the values obtained by ES-ICP. This can be explained by the fact that the calibration of RF-spectrometers uses standards with the content of elements, clearly beyond the boundaries of the proposed composition of the studied fluxes.

At the same time it is obvious that with the use of multielement standards in the ES-ICP method one can get good results even under a wide variation of components.

References

1. V.P. Afonin, et al., X-ray fluorescence analysis, Nauka, Novosibirsk, 1991.
2. H. Erhardt (editor), X-ray fluorescence analysis. Applications in plant laboratories, Metallurgiya, Moscow, 1985.
3. Karmanov, V.I. and Zagorodnyi, V.V., Zavod. Lab., 1989, No. 6, 31-36.

Table 1. Comparative evaluation of the content of components in standard flux specimens, wt.%

Components	OSTs-45			AN-20P			ANF-4		
	Standard	ES-ICP	XFA	Standard	ES-ICP	XFA	Standard	ES-ICP	XFA
SiO_2	41.7	41.1	40.6	23.0	24.0	20.5	2.06	2.21	1.38
Al_2O_3	2.14	2.33	2.00	23.9	23.1	25.6	24.6	23.5	17.3
CaO (acc. to total Ca content)	9.9	10.0	13.7	23.9	23.1	25.6	52.9	52.6	48.3
MnO	42.3	42.5	41.6	0.43	0.45	0.40	-	-	0.01
MgO	0.82	0.84	0.57	11.4	11.1	15.7	-	1.22	1.48
Fe_2O_3	0.83	0.78	0.70	0.84	0.80	0.57	0.13	0.19	0.09
K_2O+Na_2O	-	0.40	0.33	2.36	2.30	1.71	-	0.44	0.07
S	0.009	0.01	-	0.030	0.027	0.041	0.020	0.015	0.016
P	0.085	0.09	0.10	0.012	0.014	-	0.013	0.016	0.013
F	-	-	2.7	-	-	11.6	-	-	31.2
CaF_2 (acc. to F content)	-	-	5.53		-	23.8		-	64.1
CaF_2 (calculated)		6.92	-		28.3	-		70.0	-
	7.02			28.1			68.7		
CaO (from starting materials, calculated)	4.80	5.05	9.7	3.75	2.73	8.5	3.60	2.37	2.3
BaO	-	0.80	0.63	-	-	-	-	-	-
ScO	-	-	0.08	-	0.08	0.07	-	0.15	0.12